Science
AAAS

Thyroid hormone–dependent adult pigment cell lineage and pattern in zebrafish

Sarah K. McMenamin *et al.*

Science **345**, 1358 (2014);
DOI: 10.1126/science.1256251

~35 m thick, may correspond to a sequence of turbidites, as observed in other grounding zone proximal sites (*25*). The ponded morphology and acoustic stratification of the sediments support this interpretation (Figs. 1 and 4). The middle basin likely contains a sediment sequence similar to that observed in the lower basin. In its position landward of the 2001 grounding zone (Fig. 1), the deep upper basin may have existed as a subglacial lake through the Holocene (*21*).

As estimates for projected sea-level rise over the next century continue to be revised from recent Intergovernmental Panel on Climate Change forecasts, the stability of GZSs need further evaluation. Relict GZSs now observed from several offshore troughs on the Antarctic continental shelf record a time of extreme rates of sea-level change in the Quaternary (*19*, *26*, *27*). Yet, "modern" GZSs found near critical regions are interpreted to have been abandoned within recent decades, which is coincident with feedbacks in ice-shelf basal melting, grounding line recession, and ice-sheet thinning (*28*). The stability of the LIS-B with its GZS through the Holocene and their recent rapid collapse suggests strong sensitivity to surface warming. This adds to the scenario of instability now facing Antarctic glacial masses and must invigorate continued examination of GZS in spite of difficulty in access, logistical risk, and competing resources.

REFERENCES AND NOTES

1. R. B. Alley, P. U. Clark, P. Huybrechts, I. Joughin, *Science* **310**, 456–460 (2005).
2. E. C. King, R. C. A. Hindmarsh, C. R. Stokes, *Nat. Geosci.* **2**, 585–588 (2009).
3. M. Oppenheimer, *Nature* **393**, 325–332 (1998).
4. S. Anandakrishnan, G. A. Catania, R. B. Alley, H. J. Horgan, *Science* **315**, 1835–1838 (2007).
5. E. Rignot *et al*., *Geophys. Res. Lett.* **31**, L18401 (2004).
6. T. A. Scambos, J. A. Bohlander, C. A. Shuman, P. Skvarca, *Geophys. Res. Lett.* **31**, L18402 (2004).
7. P. Skvarca, H. De Angelis, A. F. Zakrajsek, *Ann. Glaciol.* **39**, 557–562 (2005).
8. T. Scambos, C. Hulbe, M. Fahnestock, in *Antarctic Peninsula Climate Variability: Historical and Paleoenvironmental Perspectives*, E. Domack, A. Burnett, A. Leventer, P. Conley, M. Kirby, R. Bindschadler, Eds., *Antarctic Research Series*, **79**, 79–92 (2003).
9. C. L. Hulbe, T. A. Scambos, T. Youngberg, A. K. Lamb, *Global Planet. Change* **63**, 1–8 (2008).
10. E. Rignot, *Philos. Trans. A Math. Phys. Eng. Sci.* **364**, 1637–1655 (2006).
11. E. Domack *et al*., *Nature* **436**, 681–685 (2005); see cover photo of issue.
12. M. Canals, R. Urgeles, A. M. Calafat, *Geology* **28**, 31–34 (2000).
13. A. Camerlenghi *et al*., *Mar. Geophys. Res.* **22**, 417–443 (2001).
14. W. Rack, H. Rott, *Ann. Glaciol.* **39**, 505–510 (2004).
15. J. Evans, C. J. Pudsey, C. O'Cofaigh, P. Morris, E. W. Domack, *Quat. Sci. Rev.* **24**, 741–774 (2005).
16. E. W. Domack, E. A. Jacobson, S. S. Shipp, J. B. Anderson, *Geol. Soc. Am. Bull.* **111**, 1517–1536 (1999).
17. M. Rebesco *et al*., *Mar. Geol.* **279**, 141–147 (2011).
18. D. E. Sugden, B. S. John, *Glaciers and Landscape: A Geomorphologic Approach* (Edward Arnold, London, 1976).
19. E. Domack *et al*., *Geomorphology* **75**, 125–142 (2006).
20. J. B. Anderson, in *The Geology of Antarctica*, R. J. Tingey, Ed. (Clarendon Press, Wotton-under-Edge, 1991), pp. 285–334.
21. T. A. Scambos, E. Berthier, C. A. Shuman, *Ann. Glaciol.* **52**, 74–82 (2011).
22. M. Rebesco, A. Camerlenghi, L. De Santis, E. Domack, M. Kirby, *Mar. Geol.* **151**, 89–110 (1998).
23. A. L. Post, M. A. Hemer, P. E. O'Brien, D. Roberts, M. Craven, *Mar. Ecol. Prog. Ser.* **344**, 29–37 (2007).
24. E. Sañé, E. Isla, M. A. Bárcena, D. J. DeMaster, *PLOS One* **8**, e52632 (2013).
25. E. W. Domack, S. E. Ishman, *Geol. Soc. Am. Bull.* **105**, 1175–1189 (1993).
26. K. McMullen *et al*., *Palaeogeogr. Palaeocl.* **231**, 169–180 (2006).
27. J. B. Anderson, *Science* **315**, 1803–1804 (2007).
28. A. Jenkins *et al*., *Nat. Geosci.* **3**, 468–472 (2010).

ACKNOWLEDGMENTS

We thank the shipboard participants, captain, and crew of cruises NBP0603 and LMG0502 and the staff at the Antarctic Marine Geology Research Facility, Florida State University. This project was supported by grants from the NSF–Office of Polar Programs (0732467 to E.D.; 0732625 to A.L.; 0732605 to S.B.) and from Italian Programma Nazionale di Ricerche in Antartide project ULISSE. The data reported in this paper are tabulated in the supplementary materials. M.R. collected and interpreted seismic reflection data aboard cruise NBP0603 and assisted with writing major portions of the manuscript. E.D. supervised collection of field data and sedimentologic core data for cruises LMG0502 and NBP0603, wrote major portions of the paper, and drafted Figs. 2 and 3. F.Z. collected, processed, and interpreted seismic reflection data aboard cruise NBP0603 and wrote sections of the paper dealing with interpretation of the reflection data. C.L. processed multibeam data, drafted Fig. 1, and wrote sections of the paper dealing with multibeam data. A.L. helped collect data aboard LMG0502 and NBP0603, analyzed diatom abundance data, and wrote sections of the paper dealing with diatom abundance and interpretation. S.B. helped collect data aboard NBP0603, collected and analyzed magnetic susceptibility data, and wrote sections of the paper dealing with physical properties of sediment cores. V.W. assisted in collecting sediment cores during LMG0502, collected color images of sediment cores during this cruise, and helped to draft portions of Fig. 2. G.H. assisted in collecting sediment cores during NBP0603, provided color images of sediment cores collected in this cruise, and helped with editing the manuscript. M.T. imported air geophysical data for interpretation of longitudinal profile of the Crane Glacier and provided editing of the manuscript. T.S. imported remote sensing data and interpretation of grounding line fluctuation before and after ice shelf collapse and assisted in writing and editing the paper. J.S. participated in collecting sediment cores and other data during LMG0502 and assisted in writing and editing the paper. E.P. was instrumental in the extensive discussion related to supplemental material dealing with ice terraces and morainal debris.

SUPPLEMENTARY MATERIALS

www.sciencemag.org/content/345/6202/1354/suppl/DC1
Materials and Methods
Figures S1 and S2
Tables S1, S2 and S3
References (*29*–*31*)

29 May 2014; accepted 1 August 2014
10.1126/science.1256697

FISH PIGMENTATION

Thyroid hormone–dependent adult pigment cell lineage and pattern in zebrafish

Sarah K. McMenamin,[1] Emily J. Bain,[1] Anna E. McCann,[1] Larissa B. Patterson,[1] Dae Seok Eom,[1] Zachary P. Waller,[1] James C. Hamill,[1] Julie A. Kuhlman,[2] Judith S. Eisen,[3] David M. Parichy[1,4]*

Pigment patterns are useful for elucidating fundamental mechanisms of pattern formation and how these mechanisms evolve. In zebrafish, several pigment cell classes interact to generate stripes, yet the developmental requirements and origins of these cells remain poorly understood. Using zebrafish and a related species, we identified roles for thyroid hormone (TH) in pigment cell development and patterning, and in postembryonic development more generally. We show that adult pigment cells arise from distinct lineages having distinct requirements for TH and that differential TH dependence can evolve within lineages. Our findings demonstrate critical functions for TH in determining pigment pattern phenotype and highlight the potential for evolutionary diversification at the intersection of developmental and endocrine mechanisms.

Vertebrates exhibit a stunning variety of pigment patterns, yet the mechanisms underlying pattern development and evolution are only beginning to be discovered. Among the most conspicuous and elaborate patterns are those of teleost fishes, which function in mate choice, shoaling, camouflage, and speciation (*1*–*3*). In the zebrafish *Danio rerio*, the adult pattern comprises dark stripes of black melanophores and a few iridescent iridophores, alternating with light "interstripes" of yellow/orange xanthophores and abundant iridophores, all within the hypodermis, between the epidermis and myotome (*4*) (Fig. 1A). Short-range and

[1]Department of Biology, University of Washington, Seattle, WA 98195, USA. [2]Genetics, Development and Cell Biology, Iowa State University, Ames, IA 50011, USA. [3]Institute of Neuroscience, University of Oregon, Eugene, OR 97403, USA. [4]Institute for Stem Cell and Regenerative Medicine, UW Medicine Research, Seattle, WA 98109, USA.
***Corresponding author. E-mail: dparichy@u.washington.edu**

long-range interactions among pigment cells are critical for patterning (*5*–*9*), and the dynamics of some of these interactions resemble those predicted by Turing models of pattern formation (*10*, *11*). Despite the emphasis on "local" pigment cell autonomous interactions, tissue-specific positional information (*7*, *8*) and "global" endocrine factors are likely required as well.

Adult pattern development involves post-embryonic differentiation and morphogenesis, potentially subject to hormonal control. By ~4 days post-fertilization (dpf), an embryonic/early larval (EL) pattern has formed with melanophore stripes and widespread, autofluorescing xanthophores (*12*) that subsequently disappear (fig. S1).

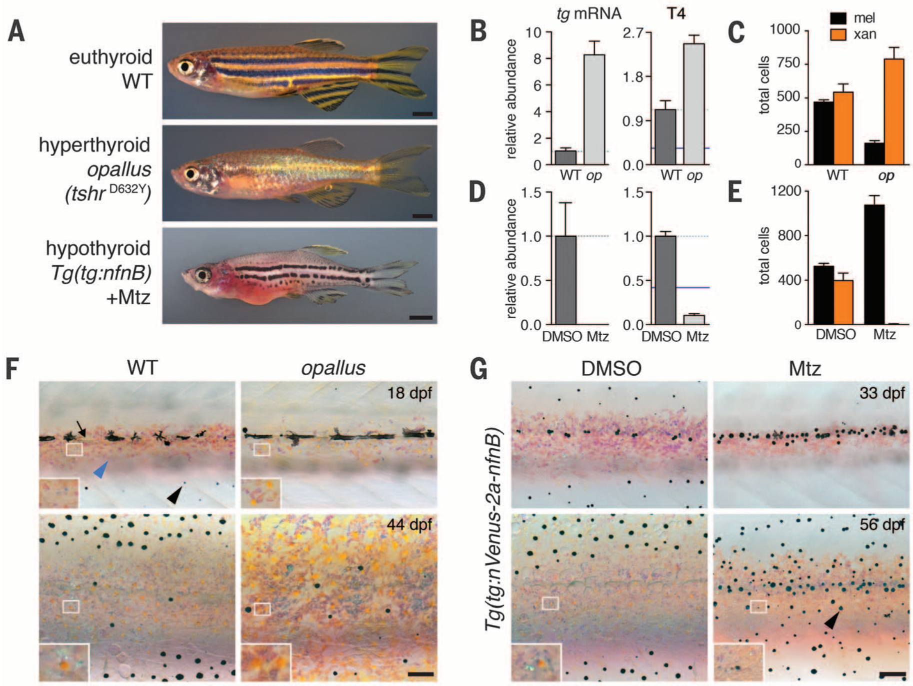

Fig. 1. TH is required for xanthophore development and melanophore repression. (**A**) Wild-type (WT), hyperthyroid, and hypothyroid phenotypes. (**B** and **C**) In *opallus*, *tg* transcript and T4 were increased [$F_{1,4} = 46$, $P < 0.005$; $F_{1,6} = 36$, $P < 0.001$; blue line, ELISA (enzyme-linked immunosorbent assay) detection limit] and there were more xanthophores but fewer melanophores [$F_{1,4} = 46$, $P < 0.005$; $F_{1,6} = 36$, $P < 0.001$; standard length (SL) 17 to 22 mm, stage J++ (*13*)]. (**D** and **E**) In thyroid-ablated fish, *tg* mRNA and T4 were undetectable ($F_{1,4} = 13$, $P < 0.05$; $F_{1,6} = 100$, $P < 0.0001$); xanthophores were missing but there were extra melanophores ($F_{1,14} = 29$, $P < 0.0001$; $F_{1,14} = 184$, $P < 0.0001$; SL 17 to 18 mm). (**F**) At 18 dpf (top), interstripe xanthophores had not yet differentiated in WT but were abundant in *opallus* (insets). Blue arrowhead, iridophores; black arrowhead, adult melanophore. By 44 dpf (bottom), *opallus* exhibited a gross xanthophore excess and severe melanophore deficiency. Fish were treated with epinephrine to contract pigment granules and facilitate counting. (**G**) Hypothyroid fish lacked xanthophores (insets) and had ectopic melanophores (black arrowhead). Note that development rate and xanthophore numbers were decreased even in dimethyl sulfoxide (DMSO) controls owing to a TH-free diet. Scale bars, 2 mm (A), 100 μm [(F) and (G)].

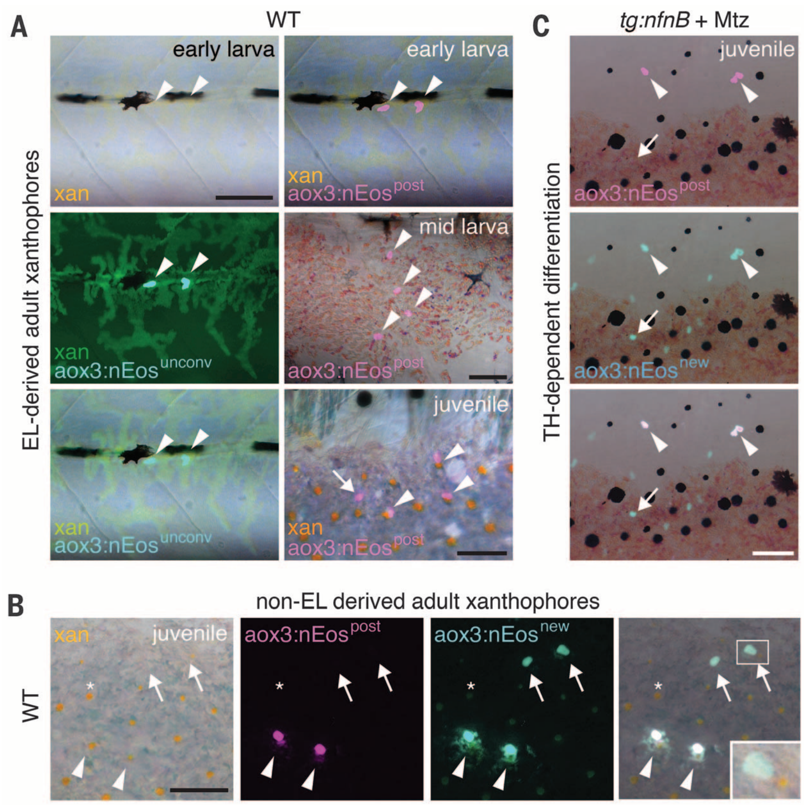

Fig. 2. Hypodermal xanthophore origins and TH dependence. (**A**) Autofluorescing *aox3*:nEos$^+$ EL xanthophores (left panels; post-photoconversion, upper right). Later, yellow pigment was absent and each cell had divided (middle right). In the juvenile, three cells redifferentiated (arrowheads) and one remained unpigmented (arrow). Overall, 86 photoconverted EL xanthophores generated 71 adult xanthophores and 78 unpigmented cells ($n = 44$ larvae); including all stages examined, marked cells had a 59% probability of dividing ($n = 82$ larvae, 190 EL xanthophores, 283 cells later). (**B**) In a juvenile in which all *aox3*$^+$ cells had been photoconverted at 5 dpf, two photoconverted EL-derived xanthophores were visible (arrowheads), but so were cells expressing only unconverted nEos (arrows), one of which had differentiated (inset); 9 of 15 juveniles had unconverted cells that developed after 5 dpf (5.8 ± 1.9, range 1 to 19 cells), of which 54% had differentiated as xanthophores. (**C**) In thyroid-ablated fish, the likelihood of photoconverted EL xanthophores (arrowheads) persisting into the juvenile did not differ from controls ($\chi^2 = 0.01$, df = 1, $P = 0.9$; Mtz, $n = 18$ larvae; DMSO, $n = 13$ larvae, 20 EL xanthophores); some cells initiated *aox3*:nEos expression only after 5 dpf (e.g., arrow). Scale bars, 60 μm.

Then, over ~4 weeks the pattern transforms into that of the adult (*13*) (movie S1). Adult melanophores and iridophores arise from "extrahypodermal" peripheral nerve–associated precursors that migrate to the hypodermis (*14*–*16*). Iridophores differentiate in the interstripe, establishing the adult pattern; melanophores initiate their differentiation more widely over the flank, and adult interstripe xanthophores appear later, in association with iridophores. Stripes gradually become more distinct as adult and residual EL melanophores in the interstripe die, are covered by iridophores, or join adult stripes, and as remaining melanophores expand and align at stripe edges (*7*, *14*, *16*–*20*). We hypothesized that the morphogenesis and differentiation of pigment cells during adult stripe development requires thyroid hormone (TH), which regulates metabolism, has cell type–specific effects, and is essential for the abrupt metamorphoses of amphibians and flatfishes (*21*–*25*).

To test TH responsiveness of pigment cells, we reared larvae in T4 (the tetra-iodinated form of TH) and observed a marked xanthophore excess and melanophore deficiency (fig. S2). These phenotypes resembled the mutant *opallus*^{b1071}, which we identified as harboring a missense mutation (Asp^{632} → Tyr) in *thyroid stimulating hormone receptor* (*tshr*) identical to a human mutation causing constitutive Tshr activity and hyperthyroidism (*26*) (Fig. 1A and fig. S3). *opallus* mutants had elevated expression of the TH precursor gene *thyroglobulin* (*tg*) and T4, more xanthophores, and fewer melanophores (Fig. 1, B, C, and F, and movies S1 and S2). Although xanthophores were the last adult pigment cell type to differentiate on the lateral flank of wild-type fish, they were the first to differentiate in *opallus* mutants (Fig. 1F and fig. S4).

To determine whether TH is required for pattern development, we sought to abolish TH production and so generated a transgenic line, *Tg(tg:nVenus-2a-nfnB)*$^{wp.rt8}$, to ablate the thyroid by metronidazole (Mtz) treatment (*27*). Fish thyroid-ablated at 4 dpf exhibited no *tg* mRNA or T4 expression as juveniles, lacked adult body xanthophores, and had excess melanophores (Fig. 1, A, D, E, and G, and movies S3 and S4). Although some xanthophores developed eventually, they were delayed relative to stage progression, which was itself retarded (figs. S4 and S5). Hypothyroid fish also had craniofacial and other defects, resembling the mutant *manet*$^{wp.r23e1}$, which we identified as a hypomorphic allele of *tshr* expressing *tg* mRNA at levels 7% of the wild type (fig. S6).

To better understand the TH dependence of xanthophores, we first identified their origins. Adult fin xanthophores and melanophores arise from stem cells (*28*), whereas adult body melanophores and iridophores arise from extrahypodermal, peripheral nerve–associated precursors (*14*–*16*); fate mapping has not revealed an extrahypodermal source of body xanthophores. We hypothesized that xanthophore precursors are already present in the hypodermis, and specifically that EL xanthophores give rise to adult xanthophores. Consistent with this idea, EL xanthophore ablation resulted in adult xanthophore deficiency (as well as defects in adult melanophore patterning; fig. S7).

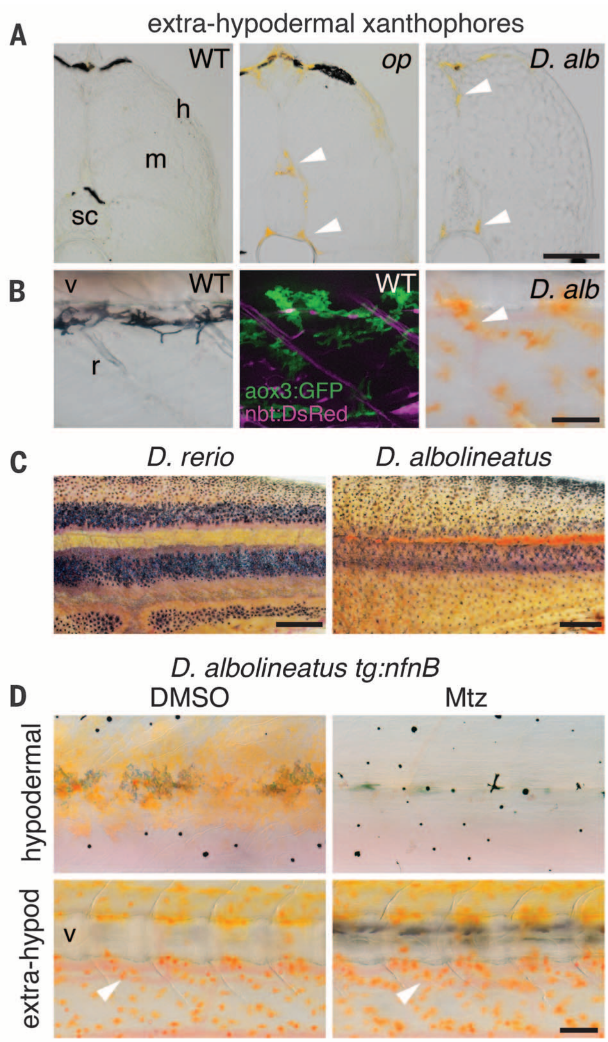

Fig. 3. Extrahypodermal xanthophores and evolution of TH dependence. (**A**) Hyperthyroid *D. rerio* (*op*) had extrahypodermal xanthophores (arrowheads). These cells were present in wild-type *D. albolineatus* (*D. alb*) as well (stage AR). sc, spinal cord; m, myotome; h, hypodermis. (**B**) Medial *aox3*:GFP^{+} cells relative to *nbt*:DsRed^{+} peripheral nerves in WT *D. rerio* (left and middle) and xanthophores (right, arrowhead) in *D. albolineatus*. v, vertebral column; r, rib. (**C**) Adult *D. rerio* and *D. albolineatus*. (**D**) Thyroid-ablated *D. albolineatus* retained extrahypodermal xanthophores (arrowheads) despite lacking most hypodermal xanthophores (fig. S12). Scale bars, 60 μm [(A) and (B)], 1 mm (C), 100 μm (D).

To test whether EL xanthophores are a source of adult xanthophores, we fate-mapped these cells with nuclear localizing photoconvertible Eos (nEos) driven mosaically by the promoter of the xanthophore pigment synthesis gene *aox3* (*17*). EL xanthophores over the lateral myotomes lost their pigment by ~8 dpf, yet persisted and proliferated (Fig. 2A, fig. S8, and movie S5). Later, photoconverted cells were found within the interstripe, where many reacquired pigment; others, in the interstripe or in melanophore stripes, failed to reacquire pigment. Thus, some adult xanthophores originate directly from neural crest–derived EL xanthophores: These cells enter a cryptic period, in which they lose pigment and proliferate; some of these cells, localizing in the interstripe, then redifferentiate during adult pattern formation. Additional cells initiated *aox3* expression only after early larval stages and thus exhibited only unconverted nEos in the juvenile, indicating a source of adult xanthophores independent of EL xanthophores as well (Fig. 2B).

In thyroid-ablated fish, EL xanthophores persisted and new *aox3*$^{+}$ cells developed, but none acquired pigment by juvenile stages (Fig. 2C). Thus, TH is not essential for survival of xanthophore lineage cells but instead promotes their differentiation. In hyperthyroid *opallus* mutants, xanthophores were more likely to divide as compared to the wild type (fig. S9 and movie S6), and differentiated not only in the hypodermis but also extrahypodermally (Fig. 3A). Stable *aox3:GFP* (green fluorescent protein) reporter lines confirmed the presence of unpigmented precursors in hypothyroid larvae and the presence of these cells within melanophore stripes of euthyroid larvae (fig. S10); *aox3*:GFP^{+} cells were also observed extrahypodermally even in the wild type (Fig. 3B). Thus, although interstripe xanthophores are the last adult pigment cell to differentiate (*7*) (fig. S4), xanthophore precursors are present throughout pattern formation, which suggests that interactions between melanophores and

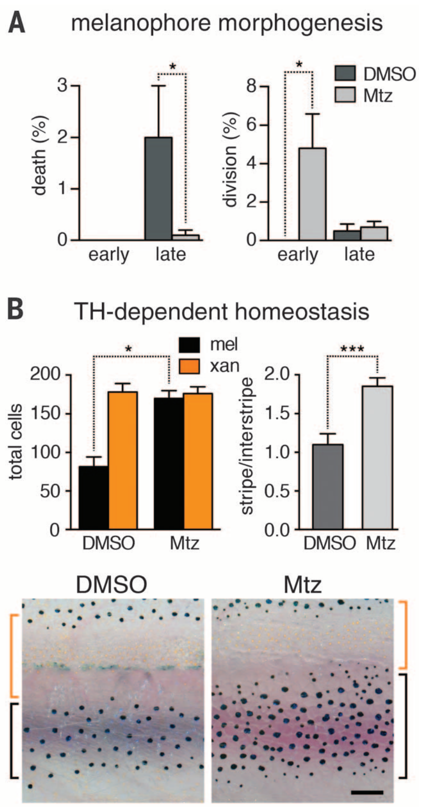

Fig. 4. TH repression of melanophores. (**A**) Melanophores of thyroid-ablated fish were less likely to die at a late stage of pattern formation (PB+; χ^2 = 35.7, df = 1, P < 0.0001) and were more likely to divide at an early stage (DR; genotype, χ^2 = 10.5, df = 1, P < 0.005; N = 45 larvae, 2510 melanophores). *P < 0.05, Tukey-Kramer post hoc test. (**B**) Thyroid ablation of juveniles resulted in more melanophores ($F_{1,19}$ = 50, P < 0.0001; *P < 0.05, Tukey-Kramer post hoc test) and wider stripes ($F_{1,19}$ = 19, P < 0.0001, ***). Scale bar, 200 μm.

xanthophores that contribute to stripe patterning (*5*, *6*, *11*) depend on the differentiative states of the interacting cells. Additionally, because xanthophore precursors were widely distributed but differentiated principally in the interstripe—where their densities increased relative to stripes (fig. S10)—a close interplay of differentiation and migration is likely important for establishing and maintaining pattern.

Effects of TH on zebrafish xanthophores led us to ask whether xanthophores of other species are TH-dependent as well. Thus, we examined *D. albolineatus*, which has an evolutionarily derived pattern in which differentiated xanthophores are intermingled with melanophores (Fig. 3C) (*29*). In this species, we found extrahypodermal xanthophores similar to those of hyperthyroid *D. rerio* (Fig. 3, A and B, and fig. S11). To see whether TH requirements are conserved, we ablated thyroids of *D. albolineatus*. These fish had hypothyroid phenotypes, yet still developed extrahypodermal xanthophores and some hypodermal xanthophores (Fig. 3D and fig. S12); this finding suggests a partial evolutionary decoupling of xanthophore development from TH in *D. albolineatus*.

In contrast to xanthophores, melanophores were more numerous in hypothyroid fish of both species, and this was particularly evident in the interstripe of *D. rerio* (Fig. 1G). To test whether TH represses proliferation or survival of these cells, we treated fish with N-phenylthiourea to retard melanization of new melanophores and facilitate tracking of previously melanized cells (*28*) (fig. S13). In euthyroid larvae, melanophores rarely divided and often died in the interstripe. In hypothyroid larvae, these cells divided frequently and were more likely to survive, whereas in hyperthyroid larvae, melanophores differentiated but many died (Fig. 4A and movies S3, S4, S7, and S8). To assess roles for TH in earlier melanophore lineage development, we examined *mitfa:GFP*^{w47}-expressing presumptive melanophore precursors (*14*). *mitfa*:GFP$^+$ cells of hypothyroid larvae were less likely to differentiate, arrive at the hypodermis, or survive (fig. S14). These defects may indicate a metabolically compromised state in the absence of TH. Thus, TH promotes hypodermal melanophore precursor abundance and differentiation while simultaneously having a greater, repressive effect on melanophore proliferation and survival.

The preceding analyses focused on pattern development, but mechanisms are also needed for pattern maintenance (*5*, *10*, *11*), and patterning mechanisms at one stage may or may not be relevant at another. To test whether TH is required for homeostasis, we ablated thyroids after the adult pattern had formed. Six months later, these fish had extra melanophores, wider stripes, and craniofacial defects, yet xanthophore numbers were unchanged (Fig. 4B and fig. S15). Thus, TH limits melanophore population expansion homeostatically but is not required by xanthophores once they have differentiated. Roles for TH in amniote melanocytes have not been well studied, but our finding that TH limits melanophore numbers may be translationally relevant, given that hypothyroidism is especially prevalent among melanoma patients (*30*, *31*).

We have identified origins of adult xanthophores distinct from those of melanophores and iridophores, revealing a previously unappreciated diversity in postembryonic neural crest lineages underlying adult pigment pattern (fig. S16A). We also found that TH represses melanophore numbers and promotes xanthophore development, yet this latter dependency has been reduced in *D. albolineatus*, raising the possibility of a new compensatory factor in this species (fig. S16B). Our results indicate that responsiveness to "global" factors such as TH should be considered along with modifications to "local" interactions in attempting to understand pattern development and evolution. The different TH dependencies of these variously colored pigment cells (fig. S5C) further suggest the potential for complex selection involving behavior, endocrine mechanisms, and diverse pigment cell lineages arising from different sources and having different fate restrictions.

REFERENCES AND NOTES

1. A. C. Price, C. J. Weadick, J. Shim, F. H. Rodd, *Zebrafish* **5**, 297–307 (2008).
2. R. E. Engeszer, G. Wang, M. J. Ryan, D. M. Parichy, *Proc. Natl. Acad. Sci. U.S.A.* **105**, 929–933 (2008).
3. O. Seehausen *et al.*, *Nature* **455**, 620–626 (2008).
4. M. Hirata, K. Nakamura, T. Kanemaru, Y. Shibata, S. Kondo, *Dev. Dyn.* **227**, 497–503 (2003).
5. D. M. Parichy, J. M. Turner, *Development* **130**, 817–833 (2003).
6. F. Maderspacher, C. Nüsslein-Volhard, *Development* **130**, 3447–3457 (2003).
7. L. B. Patterson, D. M. Parichy, *PLOS Genet.* **9**, e1003561 (2013).
8. H. G. Frohnhöfer, J. Krauss, H. M. Maischein, C. Nüsslein-Volhard, *Development* **140**, 2997–3007 (2013).
9. H. Yamanaka, S. Kondo, *Proc. Natl. Acad. Sci. U.S.A.* **111**, 1867–1872 (2014).
10. M. Yamaguchi, E. Yoshimoto, S. Kondo, *Proc. Natl. Acad. Sci. U.S.A.* **104**, 4790–4793 (2007).
11. A. Nakamasu, G. Takahashi, A. Kanbe, S. Kondo, *Proc. Natl. Acad. Sci. U.S.A.* **106**, 8429–8434 (2009).
12. R. N. Kelsh, M. L. Harris, S. Colanesi, C. A. Erickson, *Semin. Cell Dev. Biol.* **20**, 90–104 (2009).
13. D. M. Parichy, M. R. Elizondo, M. G. Mills, T. N. Gordon, R. E. Engeszer, *Dev. Dyn.* **238**, 2975–3015 (2009).
14. E. H. Budi, L. B. Patterson, D. M. Parichy, *PLOS Genet.* **7**, e1002044 (2011).
15. C. M. Dooley, A. Mongera, B. Walderich, C. Nüsslein-Volhard, *Development* **140**, 1003–1013 (2013).
16. A. P. Singh, U. Schach, C. Nüsslein-Volhard, *Nat. Cell Biol.* **16**, 607–614 (2014).
17. D. M. Parichy, D. G. Ransom, B. Paw, L. I. Zon, S. L. Johnson, *Development* **127**, 3031–3044 (2000).
18. D. M. Parichy, J. M. Turner, *Dev. Biol.* **256**, 242–257 (2003).
19. I. K. Quigley *et al.*, *Development* **131**, 6053–6069 (2004).
20. E. H. Budi, L. B. Patterson, D. M. Parichy, *Development* **135**, 2603–2614 (2008).
21. G. Van Vliet, M. Polak, *Thyroid Gland Development and Function* (Karger, Basel, Switzerland, 2007).
22. V. Laudet, *Curr. Biol.* **21**, R726–R737 (2011).
23. Y.-B. Shi, *Amphibian Metamorphosis: From Morphology to Molecular Biology* (Wiley, New York, 2000).
24. S. K. McMenamin, D. M. Parichy, *Curr. Top. Dev. Biol.* **103**, 127–165 (2013).
25. L. T. van der Ven, E. J. van den Brandhof, J. H. Vos, D. M. Power, P. W. Wester, *Environ. Sci. Technol.* **40**, 74–81 (2006).
26. A. Hébrant, W. C. van Staveren, C. Maenhaut, J. E. Dumont, J. Leclère, *Eur. J. Endocrinol.* **164**, 1–9 (2011).
27. S. Curado, D. Y. Stainier, R. M. Anderson, *Nat. Protoc.* **3**, 948–954 (2008).
28. S. Tu, S. L. Johnson, *Development* **137**, 3931–3939 (2010).
29. I. K. Quigley *et al.*, *Development* **132**, 89–104 (2005).
30. J. A. Ellerhorst, C. D. Cooksley, L. Broemeling, M. M. Johnson, E. A. Grimm, *Oncol. Rep.* **10**, 1317–1320 (2003).
31. M. Shah, I. F. Orengo, T. Rosen, *Dermatol. Online J.* **12**, 1 (2006).

ACKNOWLEDGMENTS

Supported by NIH grants R01 GM096906, R01 GM096906, and R03 HD074787 (D.M.P.), NIH grant P01 HD22486 (J.S.E.), and NIH grants F32 GM090362 and K99 GM105874 (S.K.M.). For assistance we thank O. Blackstone, T. Larson, J. Lewis, H. Majeski, E. Melancon, S. Palekha, T. Pham, A. Pruett, S. Redmond, J. Spiewak, and A. Wagner.

SUPPLEMENTARY MATERIALS

www.sciencemag.org/content/345/6202/1358/suppl/DC1
Materials and Methods
Figs. S1 to S16
Movies S1 to S8
References (*32*–*37*)

19 May 2014; accepted 6 August 2014
Published online 28 August 2014;
10.1126/science.1256251

www.sciencemag.org/cgi/content/full/science.1256251/DC1

Supplementary Materials for

Thyroid hormone–dependent adult pigment cell lineage and pattern in zebrafish

Sarah K. McMenamin, Emily J. Bain, Anna E. McCann, Larissa B. Patterson, Dae Seok Eom, Zachary P. Waller, James C. Hamill, Julie A. Kuhlman, Judith S. Eisen, David M. Parichy*

*Corresponding author. E-mail: dparichy@u.washington.edu

Published 28 August 2014 on *Science* Express
DOI: 10.1126/science.1256251

This PDF file includes:

Materials and Methods

Figs. S1 to S16

Captions for movies S1 to S8

References

Other supplementary material for this manuscript includes the following:

Movies S1 to S8

Materials and Methods

Rearing conditions

Fish stocks were reared under standard conditions at 28.5°C under 12:12 light:dark cycles. Media was changed daily for treatments with L-thyroxine (T4), 3,3',5-triiodo-L-thyronine (T3), methimazole (MMI), or N-phenylthiourea (PTU; Sigma-Aldrich). All chronic drug treatments (T4, T3 and MMI) were initiated at 4 dpf. All thyroid-ablated (Mtz-treated) and control (DMSO-treated) *Tg(tg:nVenus-v2a-nfnB)* fish were kept under TH-free conditions, fed only *Artemia* and rotifers enriched with TH-free Algamac (Aquafauna) and kept in static water tanks changed weekly.

Mutagenesis and mapping

Both *opallus*^{b1071} and *manet*$^{wp.rt8}$ were identified in forward genetic screens for mutations induced by ethyl-N-nitrosourea in AB and wik^{wp} genetic backgrounds, respectively. The semi-dominant *opallus* allele was introgressed into the highly inbred AB^{wp} genetic background and families screened for reduced penetrance of mutant phenotypes in heterozygotes. For genetic mapping, homozygous *opallus* in this background were then crossed to wik^{wp}, whereas the recessive *manet* allele was crossed to AB^{wp}. F1 *opallus* map cross fish were backcrossed to *opallus* whereas F1 map cross *manet* fish were in-crossed. From F2s, genomic DNA was extracted for each of 40 WTs and 40 mutants, pooled by phenotype and 100 bp single-end libraries constructed then sequenced on an Illumina HiSeq 2000 through the University of Oregon Genomics Core Facility at ~6x whole genome coverage. Regions of homozygosity and candidate lesions were identified with the on-line software tool SNPtrack [http://genetics.bwh.harvard.edu/snptrack *(32)*]. Variants were confirmed by Sanger sequencing and compared to pre-mutagenized haplotypes and public SNP databases.

Transgenesis and transgenic line production

Transgenesis employing *Tol2* transposase, as well as Gateway Tol2kit and other vectors followed standard procedures (*33, 34*). To ablate TH-producing thyroid follicles, we cloned 514 bp 5' to the *tg* start site and used it to drive nuclear localized Venus linked by viral 2a sequence to Ntr, encoded by *nfnB* (*27*). We generated stable lines using this construct in both *D. rerio* and *D. albolineatus*. To either ablate or fate map EL xanthophores, we cloned a 3612 bp region including the first intron of *aox3* and used site-directed mutagenesis to eliminate the native initiation codon. The fragment was then used to drive an internal amplification cassette consisting of Gal4FF (*35*), unrelated intronic spacer sequence, and a non-redundant 4xUAS [4xUAS(nr)] resistant to silencing (*36*), which was itself placed upstream of either *nVenus-2a-nfnB* or *nEos*. An additional construct for EL xanthophore ablation used BAC CH211-246M6 harboring *aox3* recombineered to contain the *nVenus-2a-nfnB* cassette. To visualize *aox3*$^{+}$ cells in non-mosaic fish we generated transgenic lines by BAC recombineering to express membrane-targeted, palmitoylated GFP; we additionally subcloned ~12 kb of this BAC and used it to generate *Tg(aox3[8.0]:palmGFP)*$^{wp.rt12}$, containing 8.0 kb of native *aox3* sequence, which exhibited an expression pattern indistinguishable from that of the BAC. An additional transgenic line, *Tg(tyrp1b:palm-mCherry)*$^{wp.rt11}$ was generated by recombineering of BAC CH211-280J15. The *Tg(nbt:DsRed)* reporter line (*7*) was generously provided by C. M. Dooley.

Nitroreductase-mediated cell ablation

To ablate thyroid follicles of *tg:nVenus-2a-nfnB D. rerio* or *D. albolineatus*, we incubated 4 dpf larvae for 4 h in either 10 mM Mtz with 1% DMSO, or 1% DMSO alone. Thyroid ablations of juveniles were performed on 4 month-old [J++, 15–17 mm standard length (SL); (*13*)] transgenic fish incubated for 24 h with Mtz or DMSO. For all thyroid ablations, treated individuals were assessed for loss of nVenus the following day; the absence of regeneration was subsequently assayed by the absence of nVenus expression. To ablate EL xanthophores, embryos were injected with *aox3:Gal4FF-4UAS(nr):nVenus-2a-nfnB* or *aox3:nVenus-2a-nfnB* (BAC), screened for robust and EL-xanthophore specific expression at 4 dpf then incubated for 24 h in 10 mM Mtz or DMSO. Fish were assessed for EL xanthophore loss the following day and evaluated for adult xanthophore deficiencies at 9.5–11 SL [stages SP–J (*13*)] when DMSO-treated controls had full complements of primary interstripe xanthophores.

Repeated image series

For time-course imaging of pigment pattern development, WT and *opallus* individuals, as well as *Tg(tg:nVenus-2a-nfnB)* DMSO-treated and Mtz-treated siblings were imaged daily beginning at stages CR/DC (~5 SL) and continuing through development of an adult pattern [J++, or the stage of anterior scale appearance (SA) for thyroid-ablated fish in which scales develop very late]. Fish were reared individually in beakers, treated with epinephrine to contract pigment granules, briefly anesthetized in MS222, imaged, then allowed to recover and returned to their beakers. Images were taken of the same region, at the middle of the flank just posterior to the anus, on a Zeiss Observer inverted compound microscope, using Zeiss Axiocam HR cameras and Axiovision software. To assess melanophore proliferation and death in the absence of new melanophore differentiation, additional *Tg(tg:nVenus-2a-nfnB)* DMSO-treated and Mtz-treated larvae were imaged daily while developing in the melanin synthesis inhibitor PTU at a concentration of 10 mM (*28*); PTU was washed out prior to the final day of imaging to reveal unmelanized melanophores.

Xanthophore fate mapping

Limiting doses of *aox3:Gal4FF-4xUAS(nr):nEos* transgene with *Tol2* transposase mRNA were injected into 1-cell embryos to yield expression in 1–30 xanthophores at 4 dpf. Single cells or small groups of cells, visually confirmed to be EL xanthophores, were then photoconverted at 4–6 dpf by 30 s exposure to epifluorescent illumination through a DAPI filter and a 20x objective with constricted aperture. Embryos were imaged before and after photoconversion to verify how many nEos^{+} yellow xanthophores had been marked. Additionally, some embryos were injected with larger doses of transgene, individuals with off-target expression discarded, and remaining larvae photoconverted by 5 min exposure to unfocussed and unfiltered mercury arc lamp illumination delivered by fiber optic cable. Photo-converted larvae were then reared individually in beakers or in small groups in tanks under dim lighting, and were examined periodically to assess the persistence and distributions of marked cells and to exclude the possibility of spontaneous photo-conversion by reference to injected, but un-converted control larvae reared identically. Batches of fish exhibiting any spontaneous photoconversion were discarded. For imaging, larvae were typically treated with epinephrine to contract pigment granules towards cell centers. Co-localization of marked nuclei and xanthophore cell bodies was verified in larvae not epinephrine treated in which pigment granules were dispersed in cell peripheries (e.g., fig. S8A).

Ex vivo time-lapse imaging

To image behaviors of melanophores, xanthophores and pigment cell precursors *ex vivo* (*14*), *Tg(mitfa:GFP)*^{w47} larvae at stage PB were rinsed with 10% Hanks medium, anesthetized and decapitated. Larval trunks were placed on 0.4 µm transwell membranes (Milipore) in glass bottom dishes containing L15 medium, penicillin/streptomycin and 10% fetal bovine serum (FBS) of a single lot containing either 20 µM T4 or the vehicle NaOH only. Because FBS was not depleted for endogenous TH, analyses here may underestimate the magnitude of differences between thyroid-intact and thyroid-ablated cell behaviors. Trunks were equilibrated for 1 h at 28.5°C, then imaged at 30 min intervals for 13.5–15.5 h on a Zeiss Observer inverted epifluorescence microscope with an Axiocam MRm camera. Z-stacks of 5–10 planes collected at 4 µm intervals were merged for final analyses. Statistical analyses of cell behaviors controlled for differences in movie duration (below). *Tg(mitfa:GFP)*^{w47} is expressed predominantly in melanophores and their precursors in contrast to other *mitfa* reporters that are expressed strongly in xanthophore precursors as well. Melanophore precursors were further identifiable at early stages of lineage development by their bipolar shape and extensive migratory activity, and at later stages of lineage development by their stellate morphology. Xanthophores and xanthophore precursors were evident by a single strongly autofluorescent spot within each cell body and considerably weaker autofluorescence in a lobate periphery. Brightfield color images taken before and after each time-lapse session were used to further verify the locations and numbers of melanized melanophores and yellow xanthophores.

Cell counts and staging

All fish were treated with epinephrine to contract pigment granules before imaging; counts were performed manually using the Cell Counter plugin feature in ImageJ. Color channel splitting and color balance modifications were used to facilitate visualization and counting of xanthophores.

For counts following TH or MMI treatments, fish were imaged at 20x or 16x magnification on a Zeiss Observer microscope; cells were counted on the flank, in the region bounded by the anterior edge of the dorsal fin and the posterior edge of the anal fin, ventral to the horizontal myoseptum. For cell counts following ablation of the thyroid in juvenile fish, individuals were treated with DMSO or Mtz (see above), reared for 6 months on a TH-free diet, then imaged at the midline posterior to the anus, on a Zeiss Observer microscope at 5x magnification. To control for changes in stripe and interstripe width, melanophores were counted only in a single stripe within the field of view; xanthophores were counted only within a single interstripe within the field of view. For *D. albolineatus*, thyroid-ablated and control fish were imaged at the midline posterior to the anus on a Zeiss Observer at 5x magnification.

To assess the effects of TH status on developmental stage and the first appearance of adult pigment cell classes, fish from multiple families were examined at numerous ages; no family was examined more frequently than every 10 days. Fish were sized and scored for the presence or absence of developmental milestones (*13*) using a Zeiss Observer inverted compound microscope and an Olympus SZX-12 stereomicroscope. A pigment cell type was scored as present if even a single cell of that type could be seen on the lateral flank of the fish.

Cell counts shown are least squares means after controlling for individual variation in SL when such variation exerted a significant effect.

<u>Quantification of *tg* expression and TH</u>

To measure *tg* expression by quantitative RT-PCR, single heads were collected and placed in RNAlater (Ambion). SLs in mm (*13*) of the decapitated fish were as follows, with comparisons in brackets: [WT, 8-8.5 SL; *opallus* 8-8.5 SL], [DMSO-treated *Tg(tg:nVenus-2a-nfnB)*, 9-10 SL; Mtz-treated *Tg(tg:nVenus-2a-nfnB)*, 9.8-10 SL], [*manet* WT siblings, 12-13 SL; *manet* 11-12 SL], [DMSO-treated *D. albolineatus Tg(tg:nVenus-2a-nfnB),* 10-12 SL PR; Mtz-treated *D. albolineatus Tg(tg:nVenus-2a-nfnB),* 9.5-11.5 SL]. RNA was extracted with Trizol (Invitrogen), treated with DNase I (Thermo Scientific), and precipitated with ammonium acetate and linear acrylamide (Ambion), then with LiCl Solution (Ambion). cDNA was synthesized with iScript cDNA Synthesis Kit (Bio-Rad). Quantitative RT-PCR was performed on an ABI StepOne Plus using SYBR Green and primers designed both to span intron–exon boundaries and to target regions of homology between *D. rerio* and *D. albolineatus* (*actb1,* ACTGGGATGACATGGAGAAGAT, GTGTTGAAGGTCTCGAACATGA; *tg*, CTCCACCCAGAGAGTTGGAC, TGTTCTTGGCTCTGCTGATG). All quantitative RT-PCRs were run with biological and technical triplicates.

To measure relative concentrations of T4 by ELISA adult male fish were collected , blotted dry and weighed, homogenized in methanol containing 1 mM 6-propyl-2-thiouracil (Sigma), then frozen at -80°C until used. Sizes and weights of the homogenized fish were as follows, with comparisons in brackets: [WT, 24-27 SL, 250-430 mg; *opallus,* 22-26 SL, 280-470 mg], [DMSO-treated *Tg(tg:nVenus-2a-nfnB),* 19-21 SL, 100-140 mg; Mtz-treated *Tg(tg:nVenus-2a-nfnB),* 19-20 SL, 130-150 mg], [DMSO-treated *D. albolineatus Tg(tg:nVenus-2a-nfnB)*, 16-18 SL, 60-100 mg; DMSO-treated *D. albolineatus Tg(tg:nVenus-2a-nfnB)*, 16-18 SL, 60-110 mg]. Two fish were combined for each sample for each comparison except the *D. albolineatus* transgenics, in which three fish were combined per sample. Homogenized samples were centrifuged for 20 minutes at 4°C, supernatant was removed and the remaining tissue was re-extracted with fresh methanol containing 6-propyl-2-thiouracil, then centrifuged a second time. Supernatants were pooled, dried by SpeedVac (~10 h), and resuspended in PBS. Samples were analyzed using a T4 ELISA kit (Diagnostic Automation) with three biological and two technical replicates for every sample, including negative controls and standards; each plate was read three times and these were averaged. Standard curves were generated using on-line analysis software [www.elisaanalysis.com]. All standard curves showed R^2 < 0.98. The empirical detection limit of each assay was calculated as the mean of the negative controls (PBS alone) plus 3 times the standard deviation of the negative controls; the detection limit of the kit was given as 0.05 μg/dL. All concentrations were normalized to the starting weight of each tissue sample.

Immunohistochemistry

To image thyroid follicles, larvae of 8.5-9.5 SL (PR–SP) were fixed in 4% paraformaldehyde, embedded in OCT Compound (Tissue-Tek), and sectioned by cryostat to 20 µm. Sections were washed with 0.3% Trition-X 100 in PBS (PBSTX), blocked with 10% heat-inactived goat serum in PBSTX, then incubated at 4°C overnight with a rabbit T4 antibody (1:1000; MP Biomedicals). Slides were then washed, incubated with a secondary antibody (goat anti-rabbit diluted 1:400, Alexa568, LifeTechnologies), stained with DAPI (1:10000), washed and imaged on a Zeiss Axioplan microscope equipped with an Axiocam MRc camera.

Image and statistical analyses

Digital images were color-balanced in Adobe Photoshop and adjusted for contrast and brightness; corresponding adjustments were made for images of both control and experimental fish. For repeated image series, images on consecutive days were rescaled and aligned by eye in Adobe Photoshop to control for overall growth during post-embryonic development.

Statistical testing used JMP 7.0 for Macintosh (SAS Institute, Cary NC). Frequency data describing behavioral outcomes for individual cells (e.g., survival vs. death) or developmental stage assignment were treated as categorical data and analyzed by single factor X^2 likelihood ratio tests or multiple logistic regression, using as factors genotype or treatment condition, size, stage, dpf, or duration of imaging as appropriate, and testing for interactions among these variables (*13*). Continuous data were evaluated by analyses of variance, typically using larval size as a covariate and testing for interactions between genotype, treatment and size. Residuals from analyses were inspected for normality and homoscedasticity; in some analyses *ln*-transformed or square root-transformed dependent variables were employed to correct for departures from model expectations.

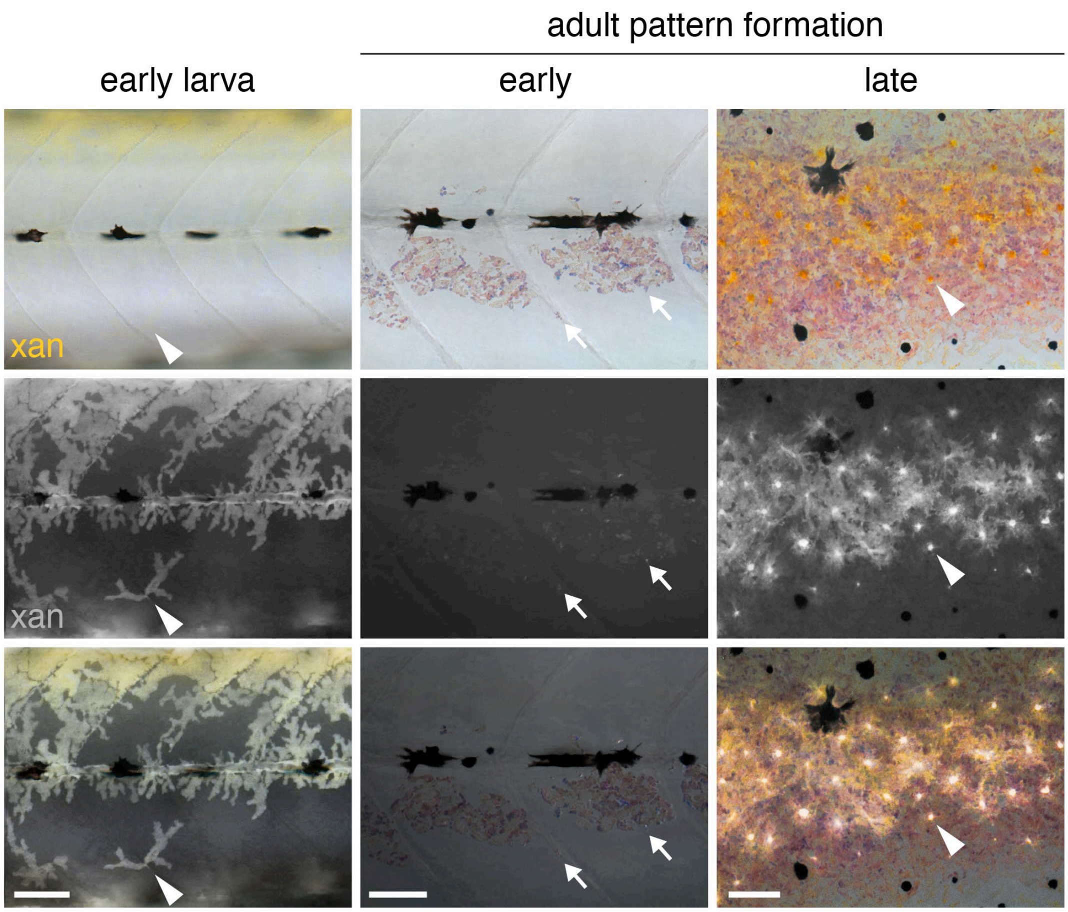

Supplementary Fig. S1. Xanthophore ontogeny over the lateral flank. Upper panels, yellow/orange xanthophore pigmentation; middle panels, xanthophore autofluorescence; lower panels, merged bright-field and fluorescence. Left panels, in the early larva (4 dpf), even lightly pigmented xanthophores were autofluorescent (e.g., arrowhead). Middle panels, at a relatively early stage of adult pigment pattern formation [DR+ (*13*); fig. S4], neither yellow xanthophores nor xanthophore autofluorescence were evident in the vicinity of the prospective interstripe (but sometimes were apparent over the dorsum); iridophores reflected epifluorescent illumination in a speckled pattern (e.g., arrows). Right panels, during late adult pattern formation (PR+), adult xanthophores had differentiated and were robustly autofluorescent (e.g., arrowhead). Fish shown were not treated with epinephrine so pigment granules were dispersed. Scale bars: 60 µm.

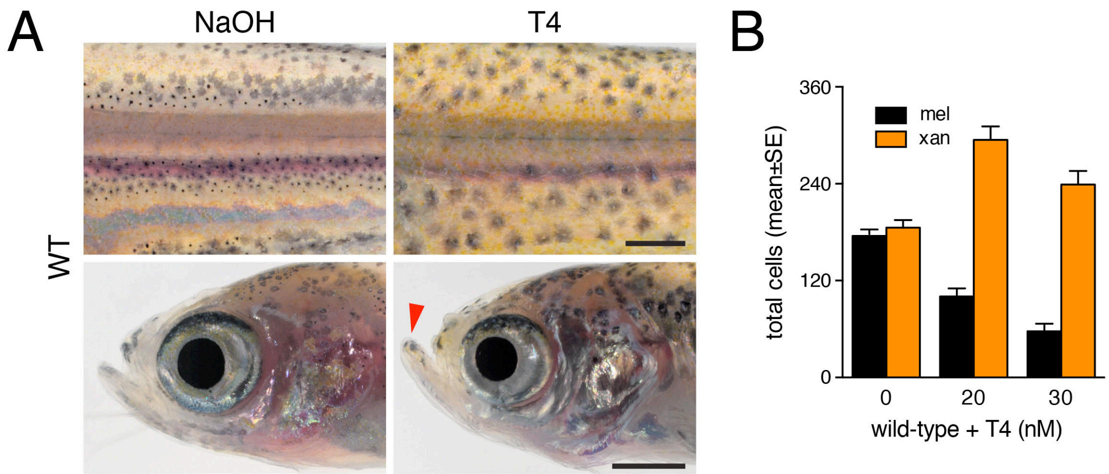

Supplementary Fig. S2. TH-responsive pigmentation and jaw phenotype. (A) WT zebrafish treated from 4 dpf with 30 nM T4 had more xanthophores, fewer melanophores, and a disorganized pigment pattern. Fish shown are juvenile stage (J+; 12.5 SL). Exogenous T4 also resulted in jaw hypertrophy (arrowhead). **(B)** Melanophores and xanthophores in WT treated with T4 (20, 30 nM) or vehicle only (0) (mel: $F_{2,32}$=73, P<0.0001; xan: $F_{2,32}$=19, P<0.0001; n=9, n=11, n=8 fish per treatment, respectively. Fish were imaged at 11–13.5 SL. Shown are least squares means±SEM after controlling for individual size variation. Scale bars: 500 µm (A, upper panels); 1 mm (A, lower panels).

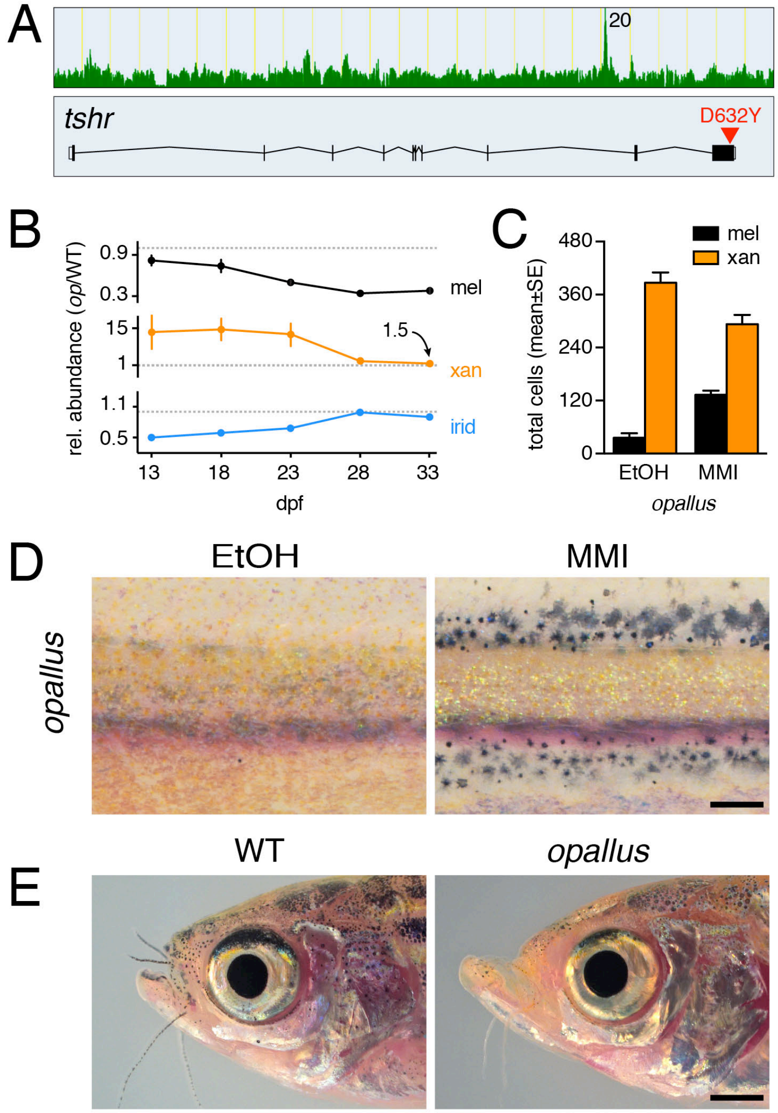

Supplementary Fig. S3. *opallus* mutant phenotype results from an activating mutation in *tshr*. (A) Bulk-segregant whole-genome re-sequencing (*31*) revealed a peak in homozygosity on chromosome 20 and a lesion in *tshr* [g1894t/D632Y, corresponding to human activating mutation D633Y (*26*)]. **(B)** Abundance of pigment cell classes in the hypodermis of *opallus* relative to WT controls (n=4 fish per genotype; shown are means±SEM, not all error bars are visible). Only hypodermal pigment cells are indicated. Dashed line, 1. **(C)** Pigment cell defects in *opallus* were rescued with methimazole (MMI), which blocks TH synthesis but can also have off-target effects (*37*). Shown are results with a relatively low dose (10 mM). Differences between vehicle and MMI treatments, both P<0.05. Fish were imaged at 18–22 SL; n=8 and n=5 fish, respectively. **(D)** Pattern recovery following treatment with 0.1 mM MMI. **(E)** *opallus* mutants displayed marked jaw hypertrophy similar to T4-treated WT fish (fig. S1). Scale bars: 200 µm (D); 1 mm (E).

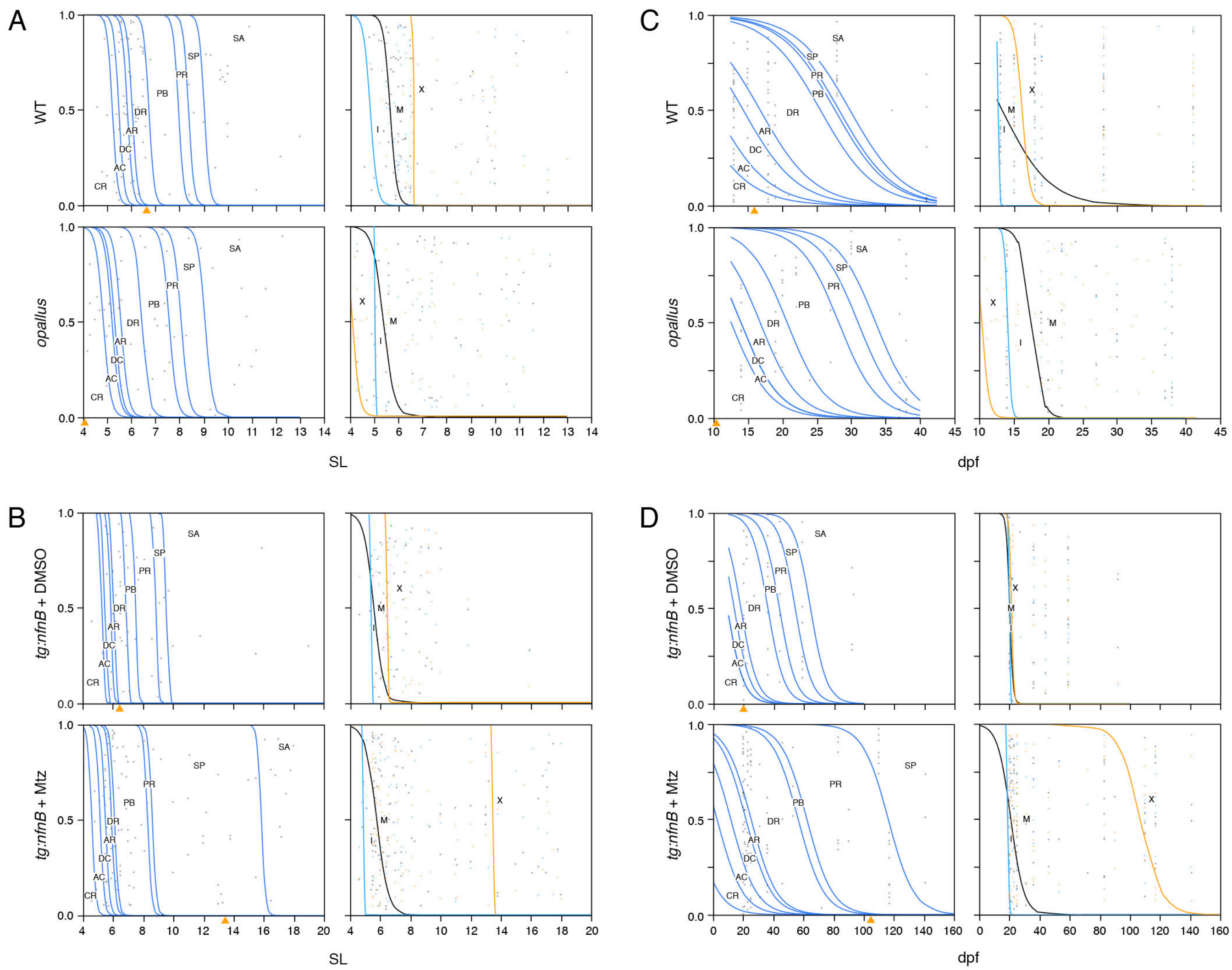

Supplementary Fig. S4. Effects of TH on developmental progression and first appearance of adult pigment cell classes. Hyperthyroid *opallus* mutants compared to (A,C) and hypothyroid Mtz-treated *Tg(tg:nVenus-2a-nfnB)* compared to euthyroid, vehicle-treated transgenic fish (B,D). Plots indicate *post hoc* probabilities (Y-axes) that fish of a given standard length (SL, in A and B) or age (dpf, in C and D) had reached a particular stage of post-embryonic development [left panels; e.g., "PB"; (*13*)], or had acquired adult pigment cells of a particular type (right panels; I, iridophores; M, melanophores; X, xanthophores). Each individual scored appears as a single point in left panels and three points (for I, M and X) in right panels. For WT in (A), for example, an individual of ~8.5 SL would have probability ~0.5 of having reached stage SP. In left panels, orange arrowheads indicate probability 0.5 of having acquired metamorphic xanthophores (representing the midpoint of probability curves in right panels), showing that xanthophore appearance was decoupled from stage. Differences in stage progression were revealed as genotype x SL or genotype x day interactions in multiple logistic regressions. WT and *opallus* did not differ in stage progression (A: X^2=2, d.f.=1, *P*=0.1; B: X^2=1, d.f.=1, *P*=0.8; WT, *n*=85 fish; *opallus*, n=55) whereas hypothyroid fish were retarded compared to controls (C: X^2=150, d.f.=1, P<0.0001; D: X^2=24, d.f.=1, P<0.0001; Mtz, n=108; DMSO, n=54). Across all stages and sizes, *opallus* mutants were more likely to have xanthophores than WT (X^2=13, d.f.=1, P<0.0005), whereas hyperthyroid fish were less likely to have xanthophores than euthyroid controls (X^2=60, d.f.=1, P<0.0001). Stages are: CR, caudal fin ray appearance; AC, anal fin condensation; DC, dorsal fin condensation; AR, anal fin ray appearance; DR, dorsal fin ray appearance; PB, pelvic fin bud appearance; PR; pelvic fin ray appearance; SP, onset of posterior squamation; SA, onset of anterior squamation (*13*)

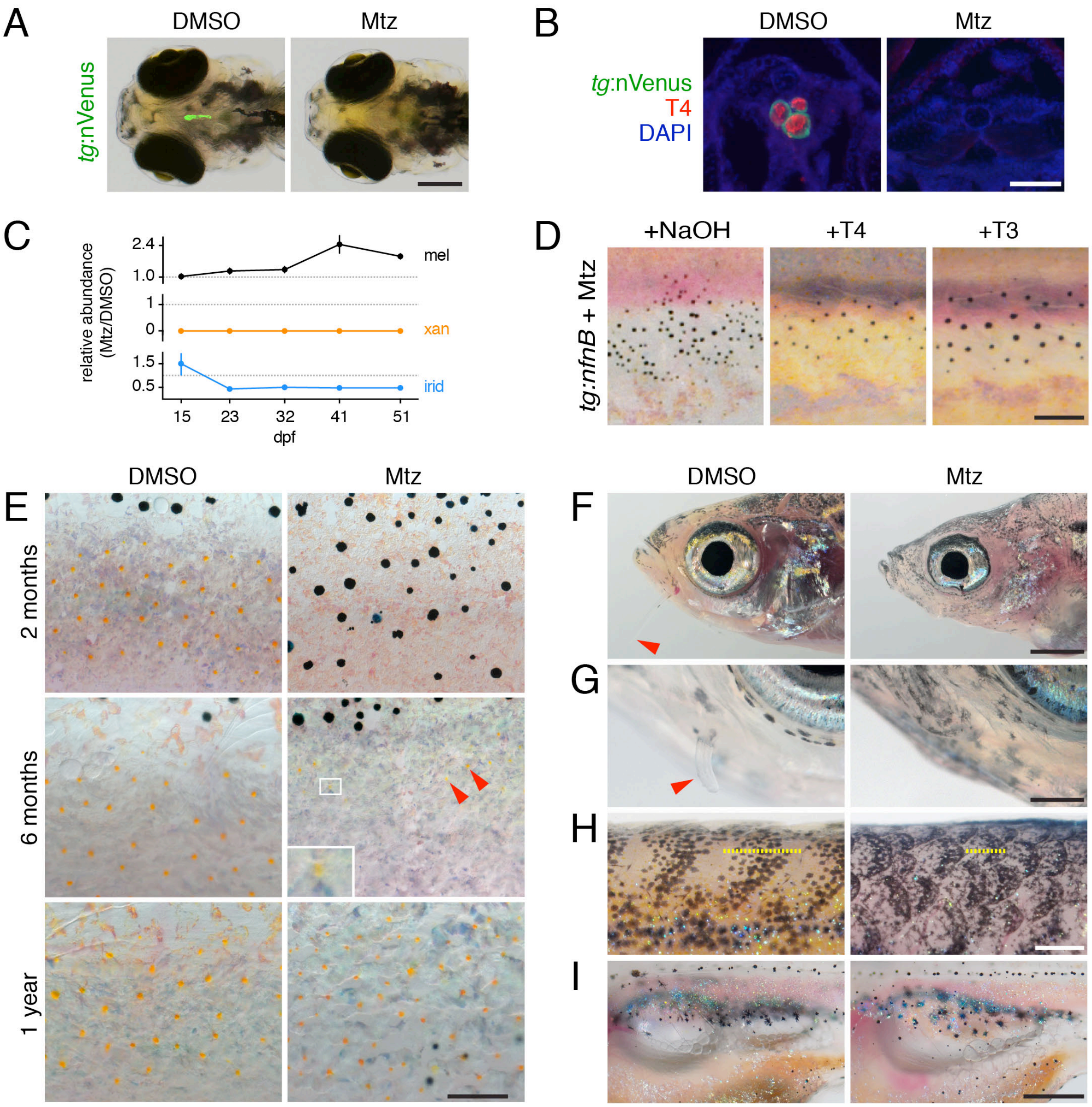

Supplementary Fig. S5. Thyroid ablation and hypothyroid phenotypes. (A) *tg*:nVenus+ thyroid follicles were missing after Mtz treatment at 4 dpf. **(B)** Absence of T4 immunoreactivity (red) and *tg*:nVenus (green) in cross sections of Mtz-treated fish; examples shown at 10 SL (stage SP). **(C)** Abundance of pigment cell classes in *Tg(tg:nvenus-2a-nfnB)* thyroid-ablated with Mtz at 4 dpf, relative to DMSO-treated sibling controls; error bars omitted for clarity (*n*=4 fish per genotype). Excess melanophores were observed by 23 dpf (stage AR–DR; fig. S4). **(D)** Hypothyroid phenotypes were rescued with low doses (5 nM) of either T4 or the genomically active, tri-iodinated form of TH, T3. (Fish were examined at 10–12 SSL; vehicle control, *n*=9 fish; T4-treated, *n*=11; T3-treated, *n*=11). **(E)** Xanthophores eventually reappeared in hypothyroid fish. Whereas none were present at 2 months, a few lightly pigmented xanthophores arose by 6 months (arrowheads and inset) and a fuller complement developed by 1 year. As xanthophores appeared, many, though not all, ectopic melanophores in the interstripe were lost. **(F–I)** Non-pigmentary phenotypes of thyroid-ablated fish. **(F, G)** Misshapen faces and absence of sensory barbels (arrowheads; adults in F and early stage of barbel development in G). **(H)** Scales developed late in hypothyroid fish (stages SP and SA in fig. S4), and were arranged more densely than in euthyroid controls; dashed yellow lines, distances between posterior edges of adjacent scales. **(I)** Swim-bladder development was markedly delayed with the transition from a single lobe to the definitive bilobate condition occurring with probability ~0.5 at ~5.5 SL (~20 dpf) in DMSO-treated fish but ~8.1 SL (~50 dpf) in Mtz-treated fish (genotype x SL interaction X^2=4.7, d.f.=1, P<0.05). Fish shown at 7.5 SL. Scale bars: 80 µm (A); 40 µm (B); 200 µm (D); 1 mm (E,F); 300 µm (G); 500 µm (H); 200 µm (I).

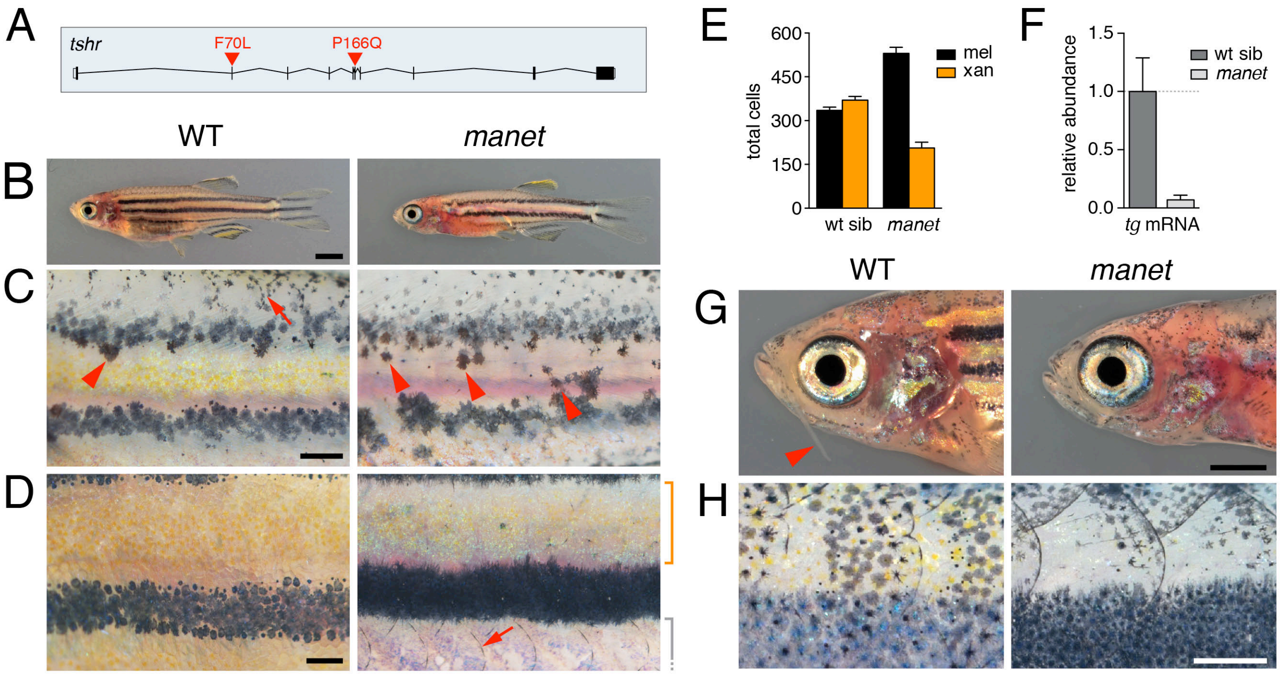

Supplementary Fig. S6. *manet* mutant phenotype results from a hypomorphic allele of *tshr*. **(A)** Lesions identified in *manet* exons encoding the extracellular region of Tshr (t201a/F70L; c497a/P166Q), N-terminal to transmembrane helices. **(B)** Adult homozygous *manet* mutant and WT sibling. **(C)** In early juveniles, a WT sibling has nearly completed stripes. Arrowhead indicates a persisting EL melanophore, identifiable by its brownish color (*19*). In *manet*, numerous EL melanophores (arrowheads) remained in the prospective interstripe along with new adult melanophores; adult xanthophores had not differentiated. Dorsally, scales had formed in WT (arrow) but not *manet*. **(D)** In adults, WT had numerous xanthophores. In *manet*, xanthophores had differentiated in the primary interstripe (upper bracket) but had not yet done so in the more ventral secondary interstripe (lower bracket), whereas melanophores developed ectopically on ventral scales (arrow). **(E)** *manet* had more hypodermal melanophores and fewer xanthophores (both P<0.001; imaged at 11–13 SL; *manet*, n=8; WT siblings, n=8; shown are least squares means after controlling for size variation). **(F)** Reduced *tg* mRNA abundance in *manet* compared to WT (*manet*/+, +/+) siblings ($F_{1,4}$=14, P<0.05). **(G)** *manet* exhibited defects in craniofacial shape and lacked barbels. **(H)** Xanthophores were missing on the late-developing scales of *manet*. Scale bars: 2 mm (A); 200 µm (C, D); 1 mm (G); 400 µm (H).

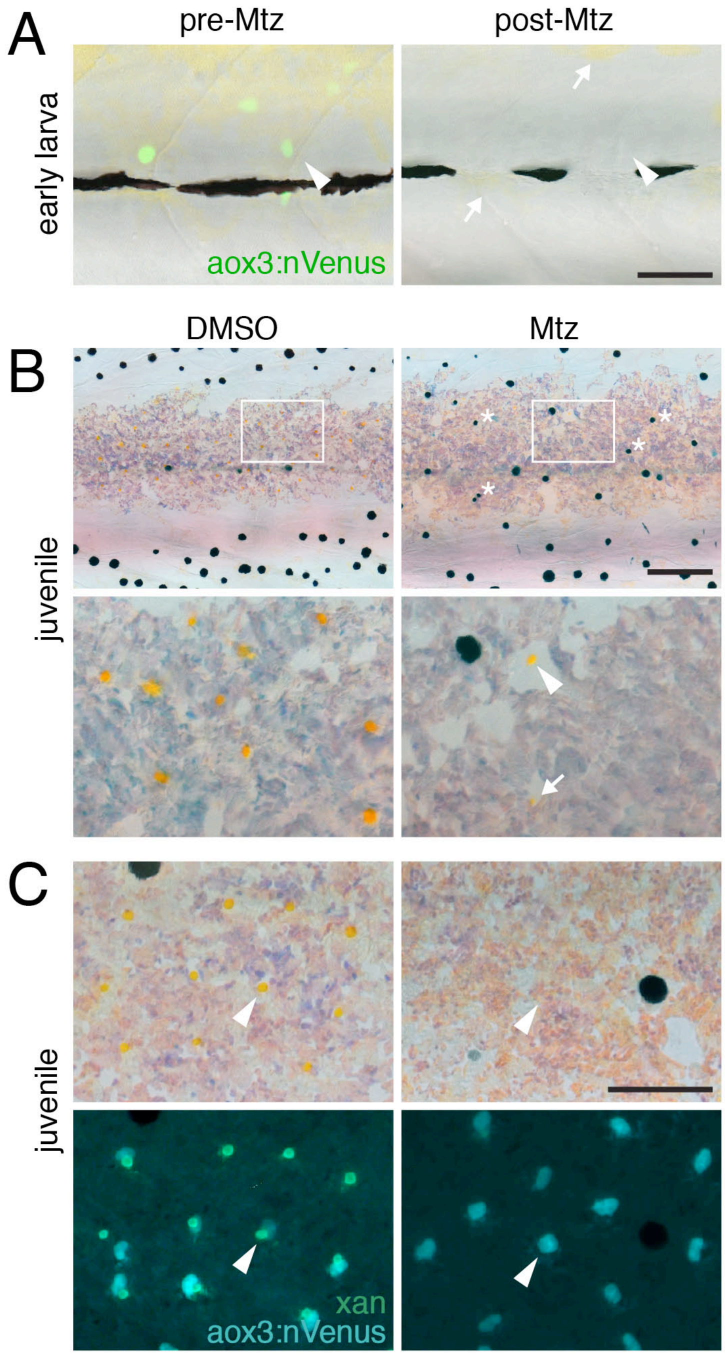

Supplementary Fig. S7. EL xanthophore ablation results in adult xanthophore deficiency. (A) Left, a 4 dpf larva injected with *aox3:Gal4FF-4xUAS(nr):nVenus-2a-nfnB* expressed Venus in nuclei of yellow xanthophores (arrowhead). Right, in the same individual after Mtz treatment, nVenus+ xanthophores were lost (arrowhead) whereas xanthophores not expressing nVenus persisted (arrows). **(B)** Near the end of adult pigment pattern formation, injected control larvae (DMSO) had normal numbers of adult xanthophores whereas those in which EL xanthophores were ablated (Mtz) had fewer adult xanthophores. Xanthophore deficiency was accompanied by the presence of ectopic melanophores in the interstripe (e.g., asterisks), demonstrating interactions between melanophores and xanthophores consistent with previous analyses (*5, 6, 11*). Lower panels, enlargements of boxed regions showing that mosaic fish did develop some xanthophores that were normally pigmented (arrowhead) or lightly pigmented (arrow; *n*=6 ablated individuals). **(C)** Control adult fish had autofluorescent xanthophores (green) and expressed *aox3*:nVenus (blue; arrowhead, left), whereas ablated fish lacked autofluorescing cells despite the presence of *aox3*:nVenus^{+} cells (arrowhead, right), consistent with an additional source of such cells independent of EL xanthophores (see main text). Scale bars: 60 µm.

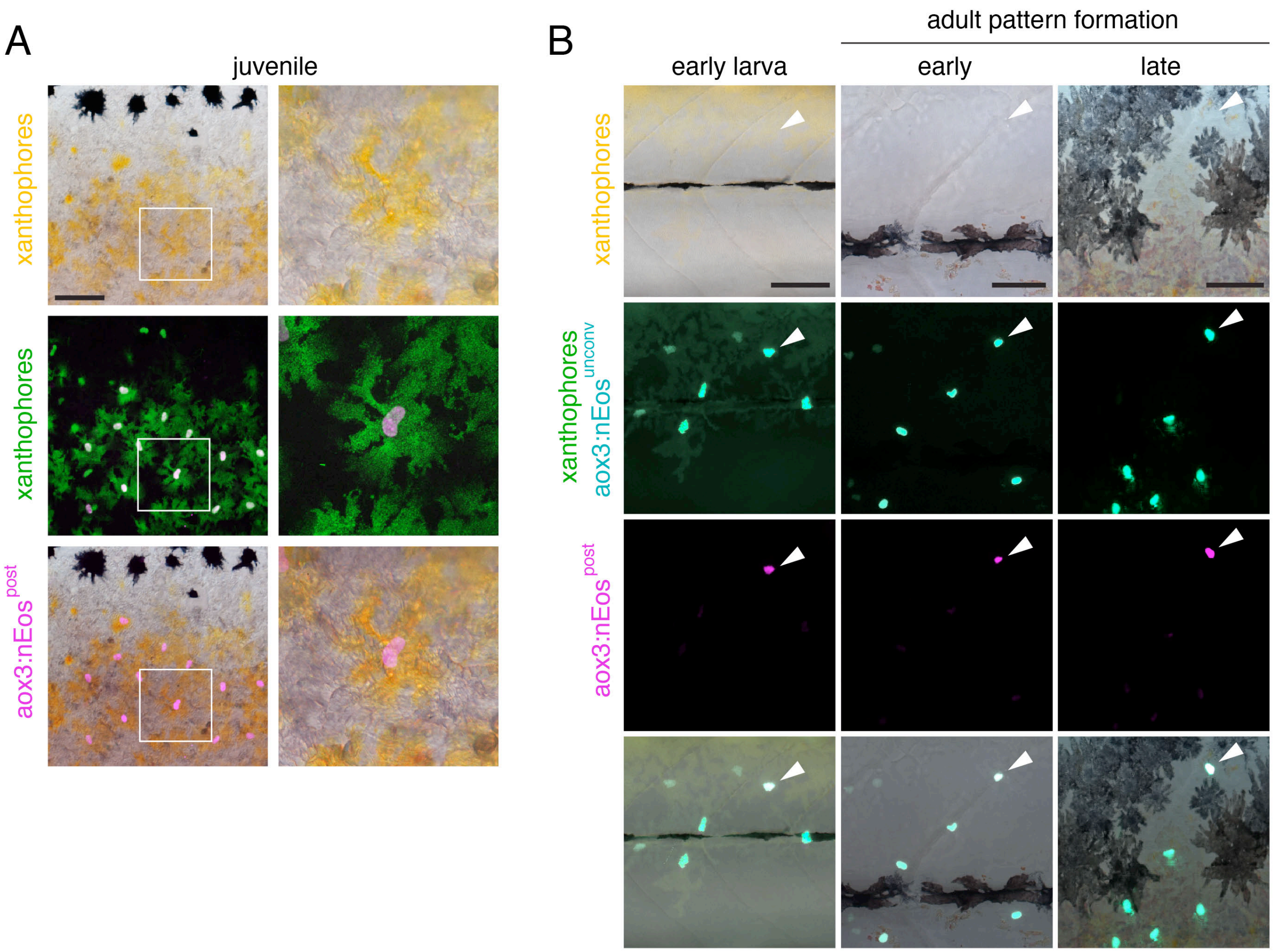

Supplementary Fig. S8. Identification of adult xanthophores derived from photoconverted *aox3*:nEos+ EL xanthophores and presence of xanthophores in adult melanophore stripes. (A) Interstripe showing numerous adult xanthophores derived from EL xanthophores that had been labeled at 5 dpf by photoconversion of nEos (*aox3*:nEos^{post}); *aox3*:nEos^{+} nuclei are contained within autofluorescent xanthophore cell bodies (movie S5). Higher magnification of boxed region at right. **(B)** Absence of spontaneous photoconversion in *aox3*:nEos^{+} EL xanthophores. In the early larva (5 dpf), several *aox3*:nEos^{+} xanthophores were visible, only one of which was photoconverted (arrowhead). At later stages, the photoconverted cell was found in the developing dorsal melanophore stripe; additional unconverted cells were present further ventrally. Scale bars: 60 µm in all panels.

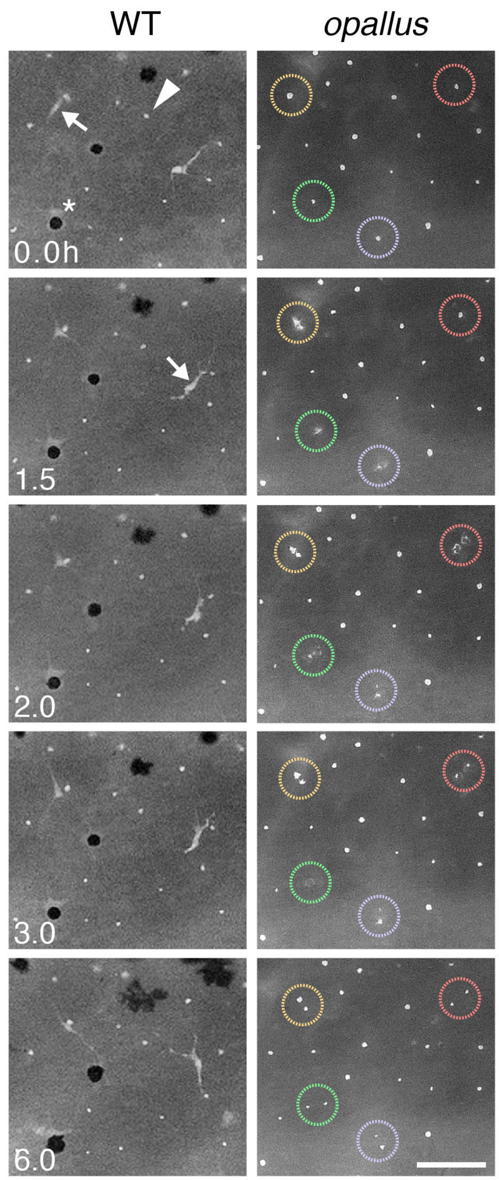

Supplementary Fig. S9. TH promotes xanthophore proliferation. Xanthophores and their precursors could be observed in time-lapse movies using the autofluorescence of pigment granules (e.g., arrowhead). Compared to WT, *opallus* exhibited 4-fold as many autofluorescent cells ($F_{1,33}$=154, P<0.0001) and individual cells were far more likely to divide during the course of time-lapse imaging (X^2=46, d.f.=1, P<0.0001; 4.0% of 2749 xanthophores examined in 9 *opallus* vs. 0.1% of 755 xanthophores in 9 WT; all at ~7.2 SL, stage PB). Colored circles indicate individual autofluorescent cells that divided over 6 h in *opallus*; no such divisions occurred in the WT example. Both carried the *mitfa:GFP*^{w47} transgene, expressed in the hypodermis primarily by melanophore precursors (*14*), readily distinguishable by their bipolar shape and extensive motility (arrowheads), or melanin at later steps in differentiation (asterisk, top left panel). Scale bar: 60 µm.

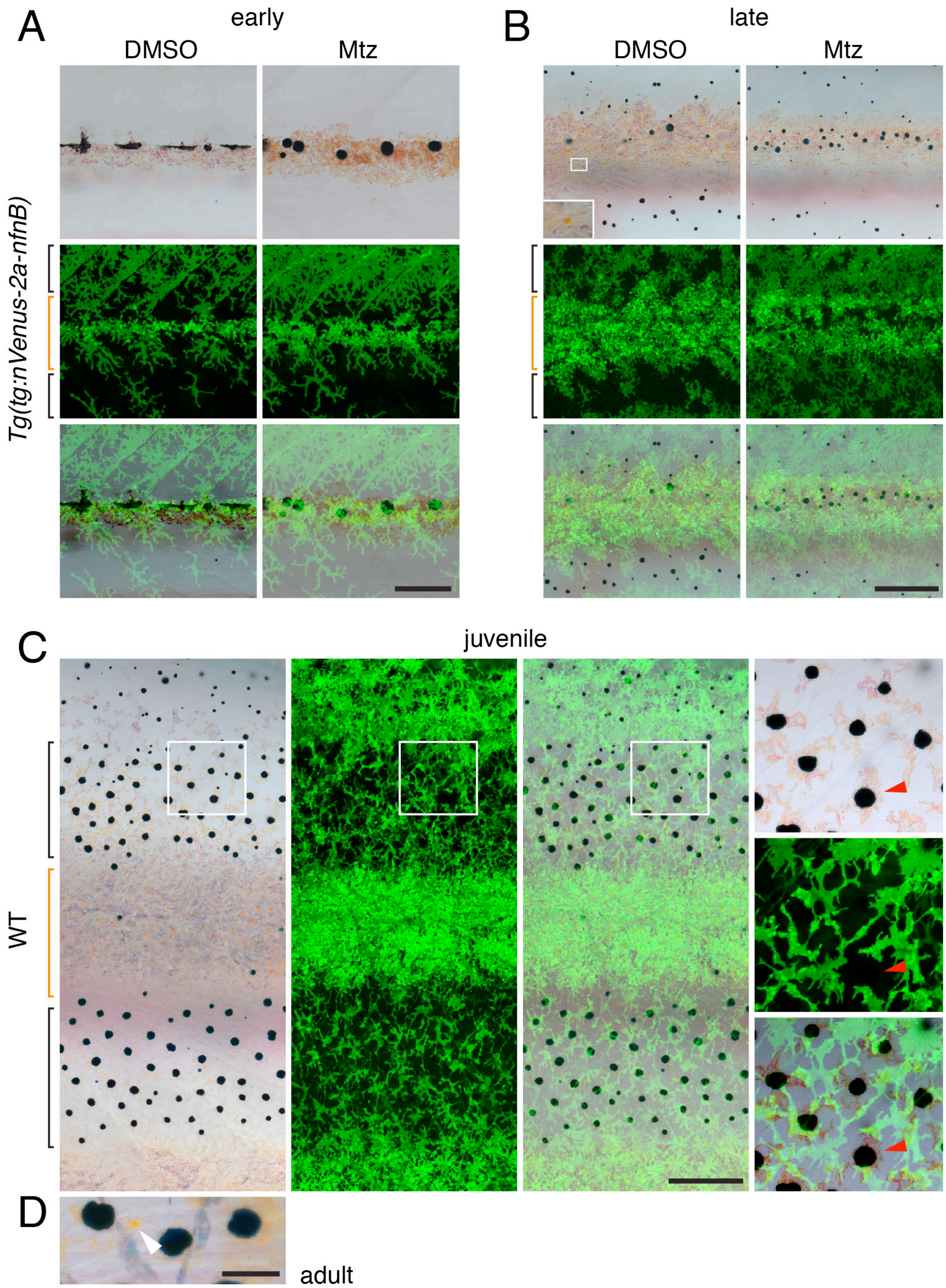

Supplementary Fig. S10. Xanthophores and xanthophore precursors in WT and hypothyroid zebrafish. Brackets show approximate locations of future stripes (black) and interstripe (orange). **(A)** In *Tg(aox3[8.0]:palmGFP)* larvae during early adult pigment pattern development [6.2 SL; stage AR (*13*)], yellow xanthophores were not evident but *aox3:*GFP+ cells (green) were abundant, especially dorsally, in both control fish (DMSO) and fish thyroid-ablated at 4 dpf (Mtz). **(B)** At a later stage of adult pigment pattern development (7.2 SL; stage PB+) *aox3*:GFP+ xanthophores had become abundant in the interstripe (inset), whereas *aox3*:GFP+ (unpigmented) cells were less abundant in prospective stripe regions. Although xanthophores were not present in thyroid-ablated fish, *aox3*:GFP+ cells were abundant, albeit dispersed more widely than in controls. **(C)** In a WT juvenile (12.0 SL; stage J) *aox3*:GFP+ cells were abundant in interstripes, where most had differentiated, but also were found within stripes, where most remained unpigmented. Insets shown at higher magnification at far right, revealing overlapping distributions of *aox3:*GFP+ cells, melanophores (melanin contracted to cell center by epinephrine treatment) and iridophores (e.g., arrowhead). **(D)** Although most *aox3*:GFP+ cells localized to melanophore stripes failed to differentiate, wild-type adult fish occassionally exhibited lightly pigmented xanthophores among stripe melanophores (arrowhead), as has been reported for adult *albino* mutant zebrafish and also in transmission electron microscopic examinations of wild-type adult zebrafish (*4*). Scale bars: 80 µm (A); 200 µm (B, C); 60 µm (D).

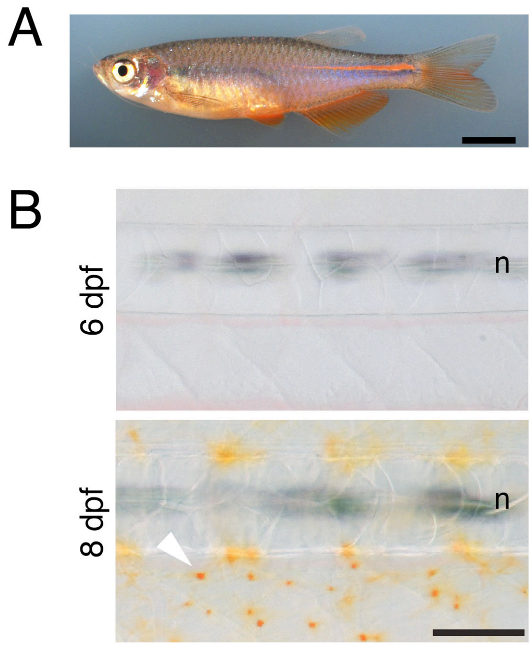

Supplementary Fig. S11. Development of extra-hypodermal xanthophores in *D. albolineatus*. (A) Externally visible pigment pattern of adult. **(B)** Extra-hypodermal xanthophores were not present in the early larva (e.g., 6 dpf) but had developed by 8 dpf. n, notochord. Scale bars: 4 mm (A); 100 µm (B).

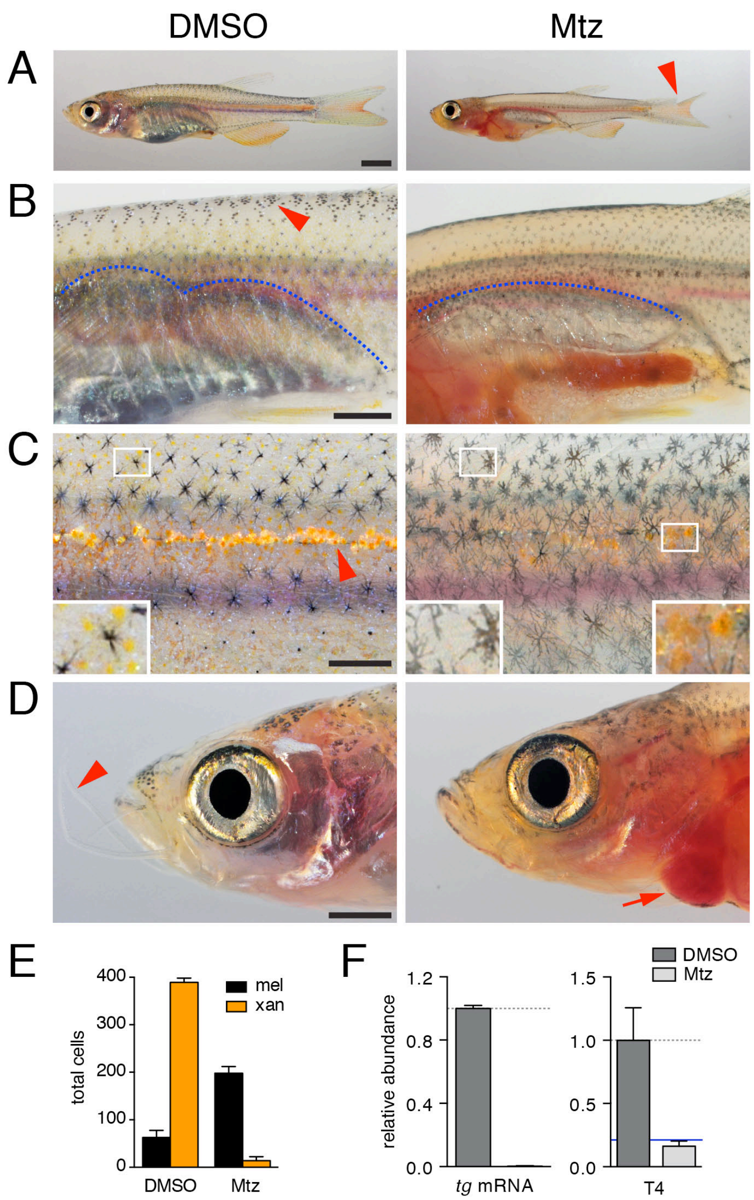

Supplementary Fig. S12. Hypothyroid phenotypes in *D. albolineatus*. (A) Juvenile hypothyroid fish (Mtz-treated at 4 dpf) were smaller than controls (DMSO), and had fragile fins prone to damage (arrowhead); this fin fragility was also observed in hypothyroid *D. rerio*. **(B)** Failure of swimbladder secondary lobe formation (outlined) and delayed scale development (arrowhead). **(C)** In thyroid-intact *D. albolineatus*, xanthophores are widespread and intermingled with melanophores (inset; arrowhead, evolutionarily reduced interstripe). In thyroid-ablated juveniles, melanophores were more abundant and xanthophores were fewer, though in contrast to *D. rerio* some xanthophores persisted, particularly in the residual interstripe (insets). **(D)** Thyroid-ablated fish also had altered head shapes, lacked barbels (arrowhead) and frequently had cardiac edema (arrow), also seen in hypothyroid *D. rerio*. **(E)** Quantification of differences in hypodermal pigment cell numbers (all P<0.0001; imaged at 19–27 SL; DMSO, n=8; Mtz, n=13). **(F)** *tg* mRNA and T4 were dramatically reduced or absent in thyroid-ablated *D. albolineatus* ($F_{1,9}$=1637, P<0.0001; $F_{1,4}$=19, P<0.05). Blue line, empirical detection limit for ELISA. Scale bars: 2 mm (A); 1 mm (B, D); 400 µm (C).

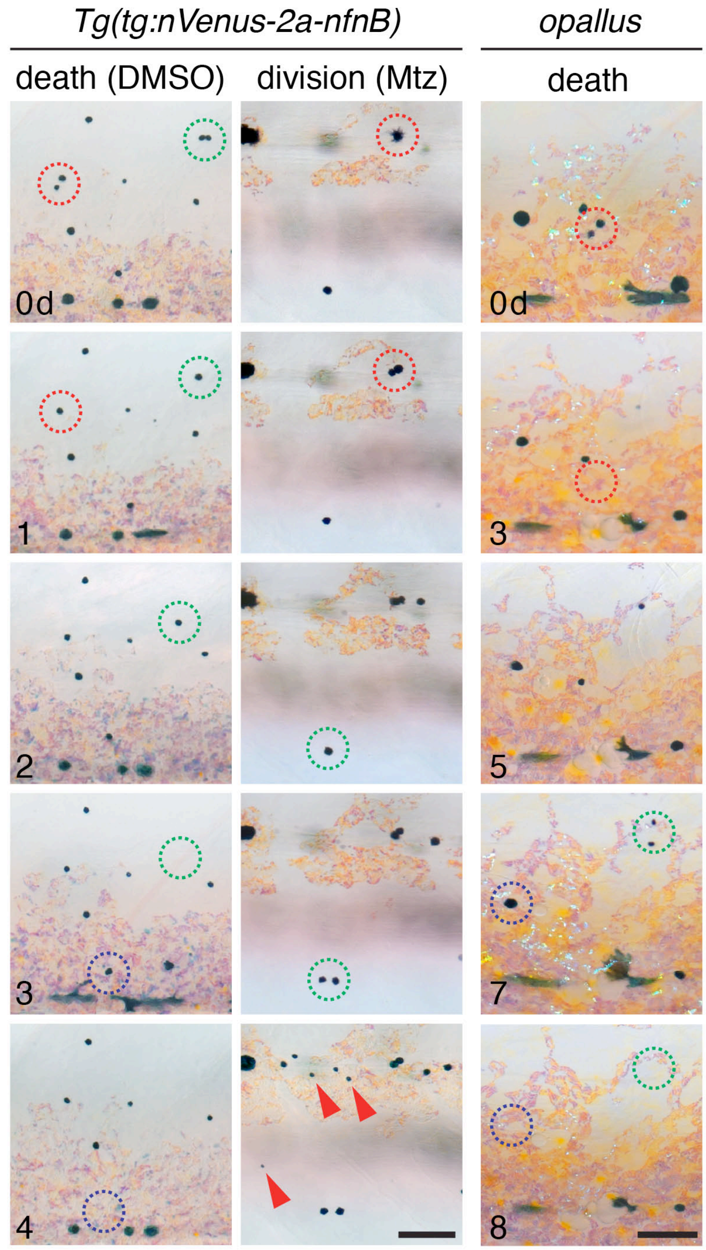

Supplementary Fig. S13. TH repression of melanophore population. Shown are repeated images of representative *Tg(tg:nVenus-2a-nfnB)* larvae treated with N-phenylthiourea (PTU), or *opallus* without PTU. Days elapsed at lower left. In euthyroid controls (DMSO) and hyperthyroid *opallus* mutants, melanophores often were lost and divided only very rarely. In thyroid-ablated larvae (Mtz) melanophores were more likely to survive and divided frequently. Colored circles indicate specific cells that either die (DMSO, *opallus*) or divide (Mtz). Arrowheads, melanophores that acquired melanin 1 d after PTU wash-out. Scale bars: 60 µm.

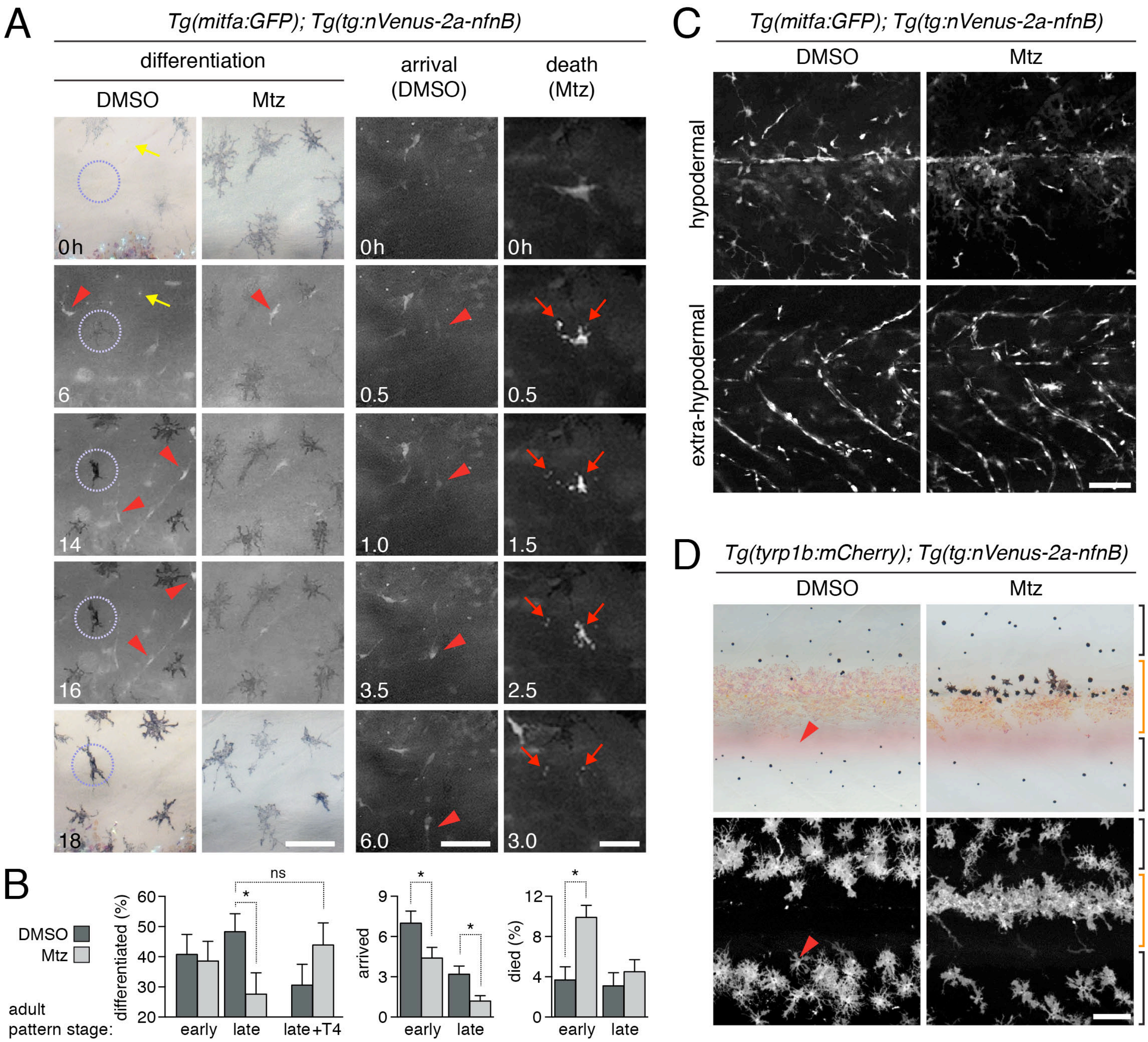

Supplementary Fig. S14. Hypothyroid defects in melanophore precursor development. (A) Frames from representative time-lapse movies, illustrating melanophore differentiation, arrival of *mitfa*:GFP$^+$ cells in the hypodermis, and *mitfa*:GFP$^+$ cell death and fragmentation. Times elapsed at lower left. Under "differentiation," top and bottom panels show starting and ending bright-field images, respectively. Circled cell acquired melanin during the time-lapse. Yellow arrow, xanthophore. Red arrowheads, highly motile, bipolar *mitfa*:GFP$^+$ presumptive early melanophore precursors. Under "arrival," a *mitfa*:GFP$^+$ cell emerged from extra-hypodermally (arrowheads; movie S7). Under "death," a *mitfa*:GFP$^+$ cell fragments, leaving behind cellular debris (arrows). **(B)** In comparison to controls (DMSO), the likelihood of stellate, *mitfa*:GFP$^+$ cells differentiating was reduced at a late stage of adult pigment pattern development (PB+) in thyroid-ablated fish (Mtz), and this defect was rescuable by acute administration of T4 during time-lapse imaging [*, P<0.05 by Tukey Kramer *post hoc* comparison; ns, not significantly different; excluding T4 treatment, effect of genotype: X^2=14.2, d.f.=1, P<0.0005; genotype x media interaction: X^2=26.6 , d.f.=1, *P*<0.0001). Thyroid-ablated trunks also had fewer *mitfa*:GFP$^+$ cells arriving in the hypodermis ($F_{1,63}$=9.1, *P*<0.0005) and an increased likelihood of *mitfa*:GFP$^+$ cells dying (X^2=35.7, d.f.=1, *P*<0.0001) at an early stage of adult pigment pattern development (DR) (*N*=4985 *mitfa*:GFP$^+$ cells scored in 101 explants from 51 larvae distributed approximately equally across stages and treatments). **(C)** *mitfa*:GFP$^+$ cells in the hypodermis and extra-hypodermally (associated with peripheral nerves (*14*). Total numbers of *mitfa*:GFP$^+$ cells did not differ in trunk explants ($F_{1,96}$=3.1, *P*=0.08) or in larvae imaged at high resolution by spinning disk ($F_{1,56}$=0.3, *P*=0.6). **(D)** Melanophores and late stage melanophore precursors were differently distributed in control and thyroid ablated fish, as revealed by *tyrp1b*:palm-mCherry. Note that cell bodies and processes were much larger than the regions containing melanin, particularly when melanin granules are contracted by epinephrine treatment as shown here. In thyroid-ablated fish, numerous melanophores were found ectopically in the interstripe region (orange bracket) and stripe regions (black brackets) were melanophore-deficient. Numbers of unmelanized *tyrp1b*:palm-mCherry$^+$ cells were highly variable among individuals and did not differ consistently between thyroid-ablated and control fish. Scale bars: 40 µm (A); 100 µm (C, D).

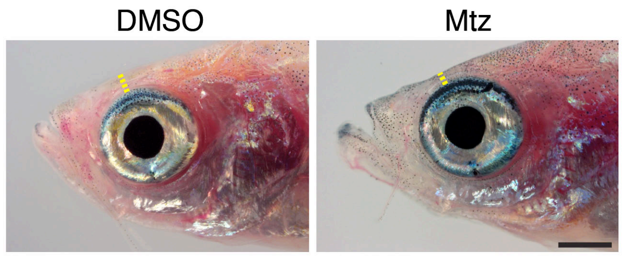

Supplementary Fig. S15. TH-dependent homeostasis of craniofacial shape in zebrafish. Fish had narrower heads 6 months after juvenile thyroid ablation (e.g., reduced distance between eye and dorso-anterior margin of head shown by dashed line). Scale bar: 1 mm.

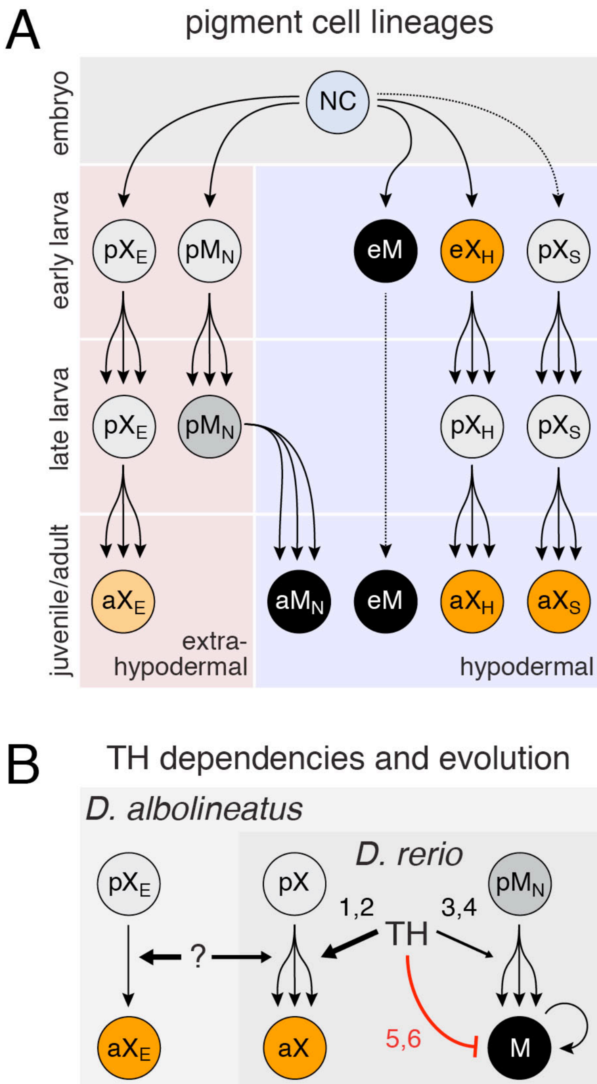

Supplementary Fig. S16. Models for pigment cell lineage relationships and TH-dependencies. (A) In the embryo, some neural crest (NC) cells develop in the hypodermis as EL xanthophores (eX_H); these proliferate and lose their pigment, but persist as cryptic precursors (pX_H), some of which re-differentiate as adult xanthophores (aX_H). Additional precursors, that may be stem cells (pX_S), also contribute xanthophores to the adult (aX_S); though depicted in the hypodermis, their earliest niche is unknown. NC cells give rise to extra-hypodermal cells (pX_E) that normally differentiate as xanthophores only in *D. albolineatus* (aX_E). Some directly NC-derived EL melanophores (eM) persist into the adult (*18-20*), but most adult melanophores arise from peripheral-nerve associated precursors (pM_N), as do iridophores (*14-16, 20*). **(B)** TH has a major role in adult xanthophore differentiation (1) and proliferation (2). TH also promotes the survival (3) and differentiation (4) of melanophore precursors, while simultaneously repressing the survival (5) and proliferation (6) of melanophores. These effects may be direct or mediated through other cell types or TH-dependent endocrine factors. In *D. albolineatus*, still-unidentified TH-independent factors (?) are likely to promote the differentiation of extra-hypodermal xanthophores and some hypodermal xanthophores, reducing the TH-dependence of this cell lineage.

Movie S1. Adult pigment pattern development in WT zebrafish. Time-lapse animation compiled for a representative individual imaged daily between stages AC–J (*13*). Images have been rescaled to control for extensive growth during this time. At the start of the animation, neural-crest derived melanophores from the EL pigment pattern were found along the horizontal myoseptum and newly differentiated adult iridophores were immediately below (blue arrow). As development proceeded, iridophores spread through the interstripe, and some EL melanophores were covered over whereas others were lost [also see (*7*)]. After iridophores developed, adult melanophores begin to differentiate (e.g., black arrow). Xanthophores differentiated later, already within the interstripe (yellow arrows).

Movie S2. Extra xanthophores and fewer melanophores during pigment pattern development of hyperthyroid *opallus* mutant zebrafish. Shown is a representative *opallus* mutant, imaged as in movie S1. At the start, lightly pigmented xanthophores were already spread over the flank, giving a faint yellow cast. Additional xanthophores (yellow arrows) could be seen as soon as iridophores appeared ventral to the horizontal myoseptum. Some adult melanophores differentiated but many were lost (dark arrows).

Movie S3. Pigment pattern formation in thyroid ablation control fish. Time-lapse animation shows a representative *Tg(tg:nVenus-2a-nfnB)* fish treated at 4 dpf with DMSO and then imaged between stages AC–SA. Adult pigment pattern development was indistinguishable from that of untreated WT fish, though somewhat protracted, due to transgenic fish being reared on a TH-free diet. Red arrows illustrate several melanophores that were lost during pattern formation; melanized debris [e.g., (*5*)] was apparent at high magnification.

Movie S4. Missing xanthophores and supernumerary, mispatterned melanophores in thyroid-ablated fish. Shown is a representative *Tg(tg:nVenus-2a-nfnB)* fish treated at 4 dpf with Mtz to ablate the thyroid and then imaged as in movie S3. The movie illustrates the lack of interstripe xanthophores and the many extra melanophores that persist in the developing interstripe.

Movie S5. nEos-marked adult xanthophore. Photoconverted *aox3*:nEos^{+} nucleus is found among autofluorescent xanthophore pigment granule. Same cell as shown in fig. S8A.

Movie S6. Xanthophore divisions in hyperthyroid *opallus* mutant. Time-lapse images from a representative *opallus* mutant shown also in fig. S13 (image interval 30 min).

Movie S7. Entry of new *mitfa*:GFP^{+} cells into the hypodermis. Shown is a representative *Tg(tg:nVenus-2a-nfnB); Tg(mitfa:GFP)* trunk (stage DR) from a thyroid-intact fish, treated at 4 dpf only with DMSO. Several *mitfa*:GFP^{+} cells emerge from extra-hypodermal regions (e.g., yellow arrowhead); note that movie is a projection of multiple Z-planes [also see: (*14*)].

Movie S8. Death of *mitfa*:GFP^{+} cells in hypothyroid mutants. Time-lapse images from the trunk of a representative *Tg(tg:nVenus-2a-nfnB); Tg(mitfa:GFP)* trunk (stage DR) from a fish that had been thyroid-ablated at 4 dpf with Mtz. Note fragmentation and rapid disappearance of fluorescent debris. Total duration, 15 h; image interval, 30 min.

References

1. A. C. Price, C. J. Weadick, J. Shim, F. H. Rodd, Pigments, patterns, and fish behavior. *Zebrafish* **5**, 297–307 (2008). Medline doi:10.1089/zeb.2008.0551

2. R. E. Engeszer, G. Wang, M. J. Ryan, D. M. Parichy, Sex-specific perceptual spaces for a vertebrate basal social aggregative behavior. *Proc. Natl. Acad. Sci. U.S.A.* **105**, 929–933 (2008). Medline doi:10.1073/pnas.0708778105

3. O. Seehausen, Y. Terai, I. S. Magalhaes, K. L. Carleton, H. D. Mrosso, R. Miyagi, I. van der Sluijs, M. V. Schneider, M. E. Maan, H. Tachida, H. Imai, N. Okada, Speciation through sensory drive in cichlid fish. *Nature* **455**, 620–626 (2008). Medline doi:10.1038/nature07285

4. M. Hirata, K. Nakamura, T. Kanemaru, Y. Shibata, S. Kondo, Pigment cell organization in the hypodermis of zebrafish. *Dev. Dyn.* **227**, 497–503 (2003). Medline doi:10.1002/dvdy.10334

5. D. M. Parichy, J. M. Turner, Temporal and cellular requirements for Fms signaling during zebrafish adult pigment pattern development. *Development* **130**, 817–833 (2003). Medline doi:10.1242/dev.00307

6. F. Maderspacher, C. Nüsslein-Volhard, Formation of the adult pigment pattern in zebrafish requires leopard and obelix dependent cell interactions. *Development* **130**, 3447–3457 (2003). Medline doi:10.1242/dev.00519

7. L. B. Patterson, D. M. Parichy, Interactions with iridophores and the tissue environment required for patterning melanophores and xanthophores during zebrafish adult pigment stripe formation. *PLOS Genet.* **9**, e1003561 (2013). Medline doi:10.1371/journal.pgen.1003561

8. H. G. Frohnhöfer, J. Krauss, H. M. Maischein, C. Nüsslein-Volhard, Iridophores and their interactions with other chromatophores are required for stripe formation in zebrafish. *Development* **140**, 2997–3007 (2013). Medline doi:10.1242/dev.096719

9. H. Yamanaka, S. Kondo, In vitro analysis suggests that difference in cell movement during direct interaction can generate various pigment patterns in vivo. *Proc. Natl. Acad. Sci. U.S.A.* **111**, 1867–1872 (2014). Medline doi:10.1073/pnas.1315416111

10. M. Yamaguchi, E. Yoshimoto, S. Kondo, Pattern regulation in the stripe of zebrafish suggests an underlying dynamic and autonomous mechanism. *Proc. Natl. Acad. Sci. U.S.A.* **104**, 4790–4793 (2007). Medline doi:10.1073/pnas.0607790104

11. A. Nakamasu, G. Takahashi, A. Kanbe, S. Kondo, Interactions between zebrafish pigment cells responsible for the generation of Turing patterns. *Proc. Natl. Acad. Sci. U.S.A.* **106**, 8429–8434 (2009). Medline doi:10.1073/pnas.0808622106

12. R. N. Kelsh, M. L. Harris, S. Colanesi, C. A. Erickson, Stripes and belly-spots—a review of pigment cell morphogenesis in vertebrates. *Semin. Cell Dev. Biol.* **20**, 90–104 (2009). Medline doi:10.1016/j.semcdb.2008.10.001

13. D. M. Parichy, M. R. Elizondo, M. G. Mills, T. N. Gordon, R. E. Engeszer, Normal table of postembryonic zebrafish development: Staging by externally visible anatomy of the living fish. *Dev. Dyn.* **238**, 2975–3015 (2009). Medline doi:10.1002/dvdy.22113

14. E. H. Budi, L. B. Patterson, D. M. Parichy, Post-embryonic nerve-associated precursors to adult pigment cells: Genetic requirements and dynamics of morphogenesis and differentiation. *PLOS Genet.* **7**, e1002044 (2011). Medline doi:10.1371/journal.pgen.1002044

15. C. M. Dooley, A. Mongera, B. Walderich, C. Nüsslein-Volhard, On the embryonic origin of adult melanophores: The role of ErbB and Kit signalling in establishing melanophore stem cells in zebrafish. *Development* **140**, 1003–1013 (2013). Medline doi:10.1242/dev.087007

16. A. P. Singh, U. Schach, C. Nüsslein-Volhard, Proliferation, dispersal and patterned aggregation of iridophores in the skin prefigure striped colouration of zebrafish. *Nat. Cell Biol.* **16**, 607–614 (2014). Medline doi:10.1038/ncb2955

17. D. M. Parichy, D. G. Ransom, B. Paw, L. I. Zon, S. L. Johnson, An orthologue of the kit-related gene fms is required for development of neural crest-derived xanthophores and a

subpopulation of adult melanocytes in the zebrafish, Danio rerio. *Development* **127**, 3031–3044 (2000). Medline

18. D. M. Parichy, J. M. Turner, Zebrafish puma mutant decouples pigment pattern and somatic metamorphosis. *Dev. Biol.* **256**, 242–257 (2003). Medline doi:10.1016/S0012-1606(03)00015-0

19. I. K. Quigley, J. M. Turner, R. J. Nuckels, J. L. Manuel, E. H. Budi, E. L. MacDonald, D. M. Parichy, Pigment pattern evolution by differential deployment of neural crest and post-embryonic melanophore lineages in *Danio* fishes. *Development* **131**, 6053–6069 (2004). Medline doi:10.1242/dev.01526

20. E. H. Budi, L. B. Patterson, D. M. Parichy, Embryonic requirements for ErbB signaling in neural crest development and adult pigment pattern formation. *Development* **135**, 2603–2614 (2008). Medline doi:10.1242/dev.019299

21. G. Van Vliet, M. Polak, *Thyroid Gland Development and Function*. (Karger, 2007).

22. V. Laudet, The origins and evolution of vertebrate metamorphosis. *Curr. Biol.* **21**, R726–R737 (2011). Medline doi:10.1016/j.cub.2011.07.030

23. Y.-B. Shi, *Amphibian Metamorphosis: From Morphology to Molecular Biology* (Wiley, New York, 2000).

24. S. K. McMenamin, D. M. Parichy, Metamorphosis in teleosts. *Curr. Top. Dev. Biol.* **103**, 127–165 (2013). Medline doi:10.1016/B978-0-12-385979-2.00005-8

25. L. T. van der Ven, E. J. van den Brandhof, J. H. Vos, D. M. Power, P. W. Wester, Effects of the antithyroid agent propylthiouracil in a partial life cycle assay with zebrafish. *Environ. Sci. Technol.* **40**, 74–81 (2006). Medline doi:10.1021/es050972c

26. A. Hébrant, W. C. van Staveren, C. Maenhaut, J. E. Dumont, J. Leclère, Genetic hyperthyroidism: Hyperthyroidism due to activating TSHR mutations. *Eur. J. Endocrinol.* **164**, 1–9 (2011). Medline doi:10.1530/EJE-10-0775

27. S. Curado, D. Y. Stainier, R. M. Anderson, Nitroreductase-mediated cell/tissue ablation in zebrafish: A spatially and temporally controlled ablation method with applications in

developmental and regeneration studies. *Nat. Protoc.* **3**, 948–954 (2008). Medline doi:10.1038/nprot.2008.58

28. S. Tu, S. L. Johnson, Clonal analyses reveal roles of organ founding stem cells, melanocyte stem cells and melanoblasts in establishment, growth and regeneration of the adult zebrafish fin. *Development* **137**, 3931–3939 (2010). Medline doi:10.1242/dev.057075

29. I. K. Quigley, J. L. Manuel, R. A. Roberts, R. J. Nuckels, E. R. Herrington, E. L. MacDonald, D. M. Parichy, Evolutionary diversification of pigment pattern in *Danio* fishes: Differential fms dependence and stripe loss in *D. albolineatus*. *Development* **132**, 89–104 (2005). Medline doi:10.1242/dev.01547

30. J. A. Ellerhorst, C. D. Cooksley, L. Broemeling, M. M. Johnson, E. A. Grimm, High prevalence of hypothyroidism among patients with cutaneous melanoma. *Oncol. Rep.* **10**, 1317–1320 (2003). Medline

31. M. Shah, I. F. Orengo, T. Rosen, High prevalence of hypothyroidism in male patients with cutaneous melanoma. *Dermatol. Online J.* **12**, 1 (2006). Medline

32. I. Leshchiner, K. Alexa, P. Kelsey, I. Adzhubei, C. A. Austin-Tse, J. D. Cooney, H. Anderson, M. J. King, R. W. Stottmann, M. K. Garnaas, S. Ha, I. A. Drummond, B. H. Paw, T. E. North, D. R. Beier, W. Goessling, S. R. Sunyaev, Mutation mapping and identification by whole-genome sequencing. *Genome Res.* **22**, 1541–1548 (2012). Medline doi:10.1101/gr.135541.111

33. A. Urasaki, G. Morvan, K. Kawakami, Functional dissection of the Tol2 transposable element identified the minimal cis-sequence and a highly repetitive sequence in the subterminal region essential for transposition. *Genetics* **174**, 639–649 (2006). Medline doi:10.1534/genetics.106.060244

34. K. M. Kwan, E. Fujimoto, C. Grabher, B. D. Mangum, M. E. Hardy, D. S. Campbell, J. M. Parant, H. J. Yost, J. P. Kanki, C. B. Chien, The Tol2kit: A multisite gateway-based construction kit for Tol2 transposon transgenesis constructs. *Dev. Dyn.* **236**, 3088–3099 (2007). Medline doi:10.1002/dvdy.21343

35. K. Asakawa, K. Kawakami, Targeted gene expression by the Gal4-UAS system in zebrafish. *Dev. Growth Differ.* **50**, 391–399 (2008). Medline doi:10.1111/j.1440-169X.2008.01044.x

36. M. G. Goll, R. Anderson, D. Y. Stainier, A. C. Spradling, M. E. Halpern, Transcriptional silencing and reactivation in transgenic zebrafish. *Genetics* **182**, 747–755 (2009). Medline doi:10.1534/genetics.109.102079

37. Y. Komoike, M. Matsuoka, K. Kosaki, Potential teratogenicity of methimazole: Exposure of zebrafish embryos to methimazole causes similar developmental anomalies to human methimazole embryopathy. *Birth Defects Res. B* **98**, 222–229 (2013). Medline doi:10.1002/bdrb.21057